

Changes in satellite retrievals of atmospheric composition over eastern China during the 2020 COVID-19 lockdowns

Robert D. Field^{1,2}, Jonathan E. Hickman¹, Igor V. Geogdzhayev^{1,2}, Kostas Tsigaridis^{1,3}, Susanne E. Bauer¹

¹NASA Goddard Institute for Space Studies, 2880 Broadway, New York, NY, USA, 10025

²Dept. of Applied Physics and Applied Mathematics, Columbia University 2880 Broadway, New York, NY, USA, 10025

³Center for Climate Systems Research, Columbia University, 2880 Broadway, New York, NY, USA, 10025

Correspondence to: Robert D. Field (robert.field@columbia.edu)

Abstract. We examined daily Level-3 satellite retrievals of AIRS CO, OMI SO₂ and NO₂, and MODIS AOD over eastern China to understand how COVID-19 lockdowns affected atmospheric composition, ~~taking into account trends that have occurred since 2005. Changes in 2020 were strongly dependent on the choice of background period since 2005 and whether trends in atmospheric composition were accounted for.~~ Over central east China during the January 23 - April 8 lockdown window, CO in 2020 was ~~12% lower than the 2005-2019 mean, but only 2% lower than what would be expected given the decreasing CO trend over that period~~ ~~between 3% and 12% lower than average depending on the background period, but not consistently less than expected from trends over different periods.~~ Similarly for AOD, 2020 was ~~between 14% and 30% lower than average~~ ~~the 2011-2019 mean~~, but not distinct from what would be expected from ~~the trends beginning after 2008~~. NO₂ in 2020 was ~~between 30% and 43% lower than the 2011-2019 mean over different background periods, but only and 17% between 17% and 33%~~ ~~lower than what would be expected given the trend over that period for trends beginning later than 2011~~. Over southern China, 2020 NO₂ was ~~between 23% and 32% lower than the mean, and between 14% and 29% lower than would be expected from different trends, not significantly different from anticipated, and CO and AOD over southern China were~~ ~~was~~ significantly higher than what would be expected, which we suggest was partly because of an active fire season in neighbouring countries. Over east central and southern China, SO₂ was higher than expected, but ~~the magnitude this~~ depended strongly on how daily regional values were calculated from individual retrievals. Future work over China, or other regions, needs to take ~~these trends~~ into account ~~the sensitivity of differences in 2020 to different background periods and trends~~ in order to separate the effects of COVID-19 on air quality from ~~recent trends previously occurring changes~~, or from variability in other sources.

1 Introduction

In an effort to control the spread of COVID-19, the Chinese government implemented a range of restrictions on movement. These led to reductions in industrial and other work related and personal activities starting January 23, 2020 in Wuhan, Hubei province, then extending to other cities and regions in the days that followed. On April 8, 2020, Wuhan was the last city to re-open after a complete lockdown that prevented most people from leaving their homes. These measures have been linked to changes in air quality. A network of surface monitoring stations in northern China observed 35% decreases in PM_{2.5} and 60% decreases in NO₂ concentrations during January 29 through February 29, as compared to the preceding three weeks; CO and SO₂ also declined (Shi and Brasseur,

39 2020). In and around Wuhan, decreases of NO₂ and PM_{2.5} were similar to regional changes, but there was a slight
40 increase in SO₂ concentrations (Shi and Brasseur, 2020). Observations by the Tropospheric Monitoring Instrument
41 (TROPOMI) showed large decreases in tropospheric NO₂ column densities over Chinese cities, on the order of
42 40% for February 11 to March 24 2020 compared to the same period in 2019, ranging from roughly 25% for cities
43 not affected by lockdown to 60% for Wuhan and Xi'an (Bauwens et al., 2020). Prospective simulations suggested
44 that meteorology may limit the effect of reduced emissions on PM_{2.5} concentrations, with Chinese cities
45 experiencing less than 20% reductions (Wang et al., 2020).

46

47 The goal of our study was to consider these changes against pollution trends in China using NASA Earth
48 Observing System data by combining several products to give a holistic view covering several emission sectors
49 that are responsible for the observed changes. Over the last 2 to 3 decades, air pollution in China appears to have
50 followed the pattern described by the Environmental Kuznets Curve (Selden and Song, 1994). This framework
51 describes a relationship in which economic growth is initially accompanied by an increase in air pollution, when
52 poverty remains widespread. But as growth continues, air pollution is expected to level off and decline as a
53 consequence of changes in social awareness of environmental degradation and the economic, political, and
54 technological capacity to limit it (Sarkodie and Strezov, 2019;Selden and Song, 1994).

55

56 Bottom-up and top-down assessments of air pollutant emissions and concentrations suggest that China has
57 followed this pattern during the era of satellite monitoring of atmospheric composition, with concentrations of
58 SO₂, NO₂, CO, and aerosol optical depth (AOD) mostly exhibiting marked and steady declines over the last
59 decade. In the case of NO₂, multi-instrument analyses, which extend the observational record beyond the lifetime
60 of a single instrument, depict a consistent regional picture of NO₂ trends in China since 1996 (Geddes et al.,
61 2016;Georgoulias et al., 2019;Wang and Wang, 2020;Xu et al., 2020). Column totals show an increasing trend
62 during the first part of the satellite record, but this trend is reversed sometime between 2010 and 2014 (Georgoulias
63 et al., 2019;Krotkov et al., 2016;Lin et al., 2019;Xu et al., 2020;Si et al., 2019;Shah et al., 2020). The trend reversal
64 has been attributed to a combination of emission control measures (Zheng et al., 2018a) and variations in economic
65 growth (Krotkov et al., 2016).

66

67 Bottom-up estimates suggest that SO₂ emissions peaked earlier, with declines starting around 2005, primarily as
68 a result of power and industrial pollution control measures as well as the elimination of small industrial boilers
69 (Sun et al., 2018;Zheng et al., 2018b). An earlier peak in SO₂ emissions is consistent with observations by multiple
70 satellite instruments, which revealed declines in SO₂ column densities since 2005 (Fioletov et al., 2016;Krotkov
71 et al., 2016;Wang and Wang, 2020;Zhang et al., 2017;Si et al., 2019).

72

73 AOD retrievals from the Along Track Scanning Radiometer instruments show a steady increase over southeastern
74 China from 1995 to 2005 (Sogacheva et al., 2020), and a decline since 2005 in the MODIS AOD (He et al., 2019).
75 The AOD peak has been argued to match either the ~2011 peak in NO₂ (Zheng et al., 2018b;Xie et al., 2019), the
76 ~2005 peak of SO₂, or to have occurred at some point in between (Ma et al., 2016), with more rapid decreases in
77 AOD after 2011 (Lin et al., 2018). The recent decrease in AOD is also seen in VIIRS retrievals (Sogacheva et al.,
78 2020). Most mitigation of direct PM_{2.5} emissions since 2010 was by industry, with residential emissions also

79 decreasing substantially (Zheng et al., 2018b). The decline in SO₂ emissions also exerted an important influence,
80 with the sulfate concentration of PM_{2.5} decreasing substantially between 2013 and 2017 (Shao et al., 2018),
81 reflecting the negative trend in SO₂ emissions.

82
83 The peak in concentrations of CO, which has an atmospheric lifetime ranging from weeks to months, is less easily
84 identified. Some studies suggest that trends have been negative potentially throughout the 21st century (Han et al.,
85 2018;Strode et al., 2016;Wang et al., 2018;Yumimoto et al., 2014;Zheng et al., 2018a), but others suggest that
86 emissions and/or column densities were increasing or flat during at least the first decade of the century (Sun et
87 al., 2018;Zhao et al., 2013;Zhao et al., 2012). The negative trend has been attributed largely to reductions in
88 emissions from industrial activity, as well as from residential and transportation sectors (Zheng et al.,
89 2018a;Zheng et al., 2018b).

90
91 In addition to these long-term trends, a number of air pollutants also exhibit strong seasonal variation in China.
92 Anthropogenic emissions of CO, SO₂, and PM_{2.5} are highest in winter, reflecting large variation in emissions from
93 the residential sector and, in the case of CO, increased emissions associated with cold-start processes in the
94 transportation sector (Li et al., 2017). Outflow of CO and AOD has a spring maximum, resulting from transport
95 of pollution, dust, and boreal biomass burning emissions (Han et al., 2018;Luan and Jaegle, 2013).

96
97 Changes in pollution over China have also come from short-term interventions. To improve air quality for the
98 2008 summer Olympics—a time when emissions in China were high and still increasing—the Chinese
99 government imposed a series of strict emissions control measures from July through September 21, 2008, which
100 were qualitatively similar to the emissions reductions expected to have accompanied the COVID-19 lockdown
101 (UNEP, 2009). As a result, NO₂ concentrations over Beijing were estimated to have declined by between 40%
102 and 60% based on satellite observations, with substantial but smaller reductions in surrounding cities often on the
103 order of 20% to 30% compared to previous years (Mijling et al., 2009;Witte et al., 2009). Regional reductions of
104 SO₂ and CO during the months of the games were estimated to be 13% and 19%, respectively (Witte et al., 2009).
105 These results are broadly consistent with on-road observations (Wang et al., 2009), but larger than some surface
106 observations comparing concentrations before and after the emission control measures were implemented (Wang
107 et al., 2010).

108
109 The COVID-related lockdowns provide a similar natural experiment to the 2008 Beijing Olympics but on the
110 other side of the Kuznets curve. The fact that the lockdowns occurred during years of decreasing air pollution
111 needs to be taken into account in attributing changes in atmospheric composition to COVID-19 lockdowns,
112 independent of the long-term trend. Following Chen et al.’s (2020) analysis of air quality improvements on
113 mortality which controlled for changes in air quality since 2016, in this study we determine whether changes in
114 2020 in satellite retrievals of CO, SO₂, NO₂ and AOD departed significantly from the expected declines associated
115 with the long-term decreases in concentrations resulting from pollution controls and technological change.

116 **2 Data and methods**

117 We used daily Level-3 (L3) retrievals from four different instruments on three different NASA Earth Observing
118 System satellites. The Atmospheric Infrared Sounder (AIRS) instrument aboard NASA's Aqua satellite is a 2300-
119 channel infrared grating spectrometer in a sun-synchronous orbit with northward equator crossing time of 1:30
120 PM. AIRS carbon monoxide (CO) profiles are retrieved with horizontal resolution of 45 km at nadir, in a swath
121 of width 30 fields-of-view or about 1600 km. The retrieval uses a cloud-clearing methodology providing CO with
122 sensitivity that peaks around 500 hPa, with ~0.8-1.2 degrees-of-freedom-of-signal for 50-70% of scenes. More
123 sampling and higher information content is obtained in clear scenes (Warner et al., 2013). We used the daily
124 version 6 (AIRS3STD.006) product.

125

126 The Ozone Monitoring Instrument (OMI) aboard NASA's Aura satellite was launched in July 2004, and has a
127 local equator-crossing time of roughly 13:45. OMI is a nadir-viewing spectrometer, which measures solar
128 backscatter in the UV-visible range (Krotkov, 2013). We used NASA's L3 tropospheric NO₂ column density
129 Standard Product v3 (OMNO2d_003), and the OMI Principal~~al~~ Components Analysis Planetary Boundary Layer
130 (PBL) SO₂ product (OMSO2e_003), which grid retrievals to 0.25° resolution (Krotkov et al., 2017; Li et al., 2013).
131 Both products are cloud-screened; only pixels that are at least 70% cloud-free are included in the NO₂ product,
132 and those that are at least 80% cloud-free are included in the SO₂ product. The NO₂ product relies on air mass
133 factors (AMFs) calculated with the assistance of an atmospheric chemical transport model and are sensitive to
134 model representations of emission, chemistry, and transport data. Instead of AMFs, the SO₂ product uses
135 spectrally-dependent SO₂ Jacobians, but can be interpreted as having a fixed AMF that is representative of
136 summertime conditions. We applied basic transient SO₂ plume filtering, excluding retrievals with SO₂ > 15 DU
137 (Wang and Wang, 2020).

138

139 Because our trend analysis uses a seasonal mean as the response variable, we assume that random errors cancel
140 out, leaving only systematic errors, which do not contribute to uncertainty in the trend analysis. Systematic errors
141 in the OMI NO₂ product have an uncertainty of 20% (McLinden et al., 2014) and are associated with AMFs and
142 tropospheric vertical column contents. The OMI NO₂ products use an implicit aerosol correction to account for
143 the optical effects of aerosols, but retrievals can be biased when aerosol loading is extreme (Castellanos et al.,
144 2015). Under these conditions, the OMI NO₂ retrieval is biased low by roughly 20 to 40% (Chimot et al., 2016).
145 Note that any aerosol-related error would have the potential effect of underestimating the magnitude of decreases
146 in NO₂ column densities when comparing 2020 to previous years. Additional bias in the NO₂ product may be
147 introduced due to the reliance on nearly cloud-free pixels, in which greater sunlight may induce higher
148 photochemical rates. For example, the current NO₂ product is biased roughly 30% low over the Canadian oil sands
149 (McLinden et al., 2014). The level-2 OMI- NO₂ product has been validated against in situ and surface-based
150 observations showing good agreement (Lamsal et al., 2014). The use of fixed Jacobians in the SO₂ product
151 introduces systematic errors of 50 to 100% for cloud-free observations (Krotkov et al., 2016).

152

153 Starting in 2007, the quality of level 1B radiance data for some OMI viewing directions has been affected, known
154 as the row anomaly. The L3 products used here exclude all pixels affected by the row anomaly from each
155 observation, but the locations of the row anomaly pixels were dynamic between 2007 and 2011, which could

156 affect any comparisons including those years. Since 2011, the pixels affected by the row anomaly problem are the
157 same, so comparisons for data only since 2011 are not affected by changes in the row anomaly.

158

159 Moderate Resolution Imaging Spectroradiometer (MODIS) sensors observe the Earth from polar orbit, from Terra
160 satellite since 2000 and from Aqua since mid 2002. In this study we use MODIS-derived AOD at 550nm obtained
161 by merging Dark Target and Deep Blue retrievals (Sayer et al., 2014). Specifically, we use the
162 Deep_Blue_Aerosol_Optical_Depth_550_Land_Mean field over land and the over ocean
163 AOD_550_Dark_Target_Deep_Blue_Combined_Mean the from Collection 6.1 L3 Gridded products MYD08 and
164 MOD08 (Hubanks et al., 2019), though very few retrievals over ocean are included in our analysis. L3 values are
165 computed on $1^\circ \times 1^\circ$ spatial grid from L2 AOD products with resolution of 10x10 km. Over land 66% of MODIS-
166 retrieved Dark-target AOD values were shown to be $\pm 0.05 \pm 0.15 \times \text{AOD}$ AERONET-observed values, with high
167 correlation ($R = 0.9$) (Levy et al., 2010). Around 78% of the Deep Blue retrievals are within the expected error
168 range of $\pm 0.05 \pm 0.20 \times \text{AOD}$ (Sayer et al., 2013). MODIS AOD data have been extensively used by the modeling
169 and remote sensing scientific communities and inter-compared with a wide range of satellite AOD products (see
170 Schutgens et al. (2020) and references therein).

171

172 We analyzed these retrievals over two large regions (Fig. 1). Central east China was comprised of Shaanxi, Hubei,
173 Anhui, Jiangsu, Shanxi, Henan, Hebei, Shandong, Beijing, and Tianjin provinces. Southern China was comprised
174 of Guizhou, Guangxi, Hunan, Jiangxi, Guangdong, Fujian and Zhejiang provinces. Daily mean quantities were
175 calculated across all valid retrievals falling within the provinces comprising the regions. For the OMI NO₂
176 columns, individual retrievals were weighted by the L3 'Weight' field, which is proportional to the fraction of the
177 grid cell with higher-quality retrievals, identified as those have less than 30% cloud fraction and not affected by
178 the row anomaly problem. We also calculated the daily value from the median of all retrievals, to understand
179 whether individual high values (mainly SO₂) had any effect on the significance of trends or differences between
180 2020 and different background periods. Monthly averages were calculated from the daily regional averages, with
181 each day weighted in the monthly average by the number of valid retrievals so as to not overrepresent days with
182 little satellite coverage or significant cloud cover. The monthly data were used to visually identify COVID-19
183 related changes against background seasonality and trends since 2005.

184

185 We examined the difference in the distribution of daily data during the 2020 January 23 to April 8 lockdown
186 period to the same period during previous years since 2005. We compared 2020 to 2019, to different background
187 periods ending in 2019 over which trends were consistent, and to the expected value for 2020 estimated from
188 these trends over different background periods. We tested the significance of these differences using bootstrap
189 resampling (Efron and Gong, 1983) with a resampling size of 2000. Given the uncertainty and uneven nature of
190 trends over different parts of China from previous studies, we identified the start of existing long-term trends for
191 each species by conducting linear regressions of the change in the four quantities over time for possible start years
192 of 2005 to 20152018. Each trend was estimated from the start year in this range until 2019. We selected the start
193 year for the most significant trend and used that trend for comparisons to 2020 data.

194

195 We also considered how the analysis depended on how the lockdown period was defined. Emissions and pollution
196 can decrease during the Chinese New Year holidays (Chen et al., 2020), which started as early as January 23 in
197 2012 and as late as February 19 in 2015, complicating COVID-19 related analyses of atmospheric composition
198 over China (Bauwens et al., 2020;Chen et al., 2020). The timing and extent of lockdowns also varied between
199 provinces and we assume that ‘slowdowns’ could have happened before or after stricter, official lockdowns. For
200 example, ground and air transportation remaining below lockdown levels nationally at least through April 14,
201 2020 (International Energy Agency, 2020). Excluding the holiday period from all years is a straightforward
202 approach to excluding any New Year holiday effects but will exclude simultaneous lockdown effects during the
203 initial, and presumably most strict, stages of the lockdown. Rather than specifying different combinations of New
204 Year holiday period and provincial-level lockdown timing, we used January 23-April 8 as our baseline period
205 (which will include all holiday periods since 2005), but examined the sensitivity of the statistics to the length of
206 the lockdown period, namely a longer lockdown period beginning one week earlier and one week later, and a
207 shorter lockdown period for February only. In interpreting the data, we put more confidence in 2020 differences
208 that were insensitive to these choices.

209 **3 Results**

210 **3.1 Regional patterns and seasonality**

211 [Figure 2](#)[Figure 2](#) shows the 2020 –2019 differences over China during the January 23-April 8 lockdown period
212 for the four satellite-retrieved quantities. There were decreases of 5-10 ppbv in AIRS CO over central east China
213 (Fig. 2a) and increases of 20-25 ppbv over southern China in 2020 compared to 2019. The increase in southern
214 China is adjacent to a stronger positive CO anomaly over the upper Mekong regions of Myanmar, Thailand and
215 Laos. There were no coherent regional changes in OMI SO₂ (Fig. 2b), but rather smaller localized difference of
216 either sign. There were decreases in NO₂ (Fig. 2c) across central east China exceeding 8×10^{15} molec cm⁻²
217 coincident with the weaker decrease in CO. Over southern China, there were comparable differences over
218 Guangdong province, with smaller differences elsewhere. There was a decrease in MODIS AOD (Fig. 2d) in
219 central-east China coincident with the decreases in CO and NO₂, but smaller in magnitude. There was a region of
220 higher AOD in and northeast of the upper Mekong region coincident with the CO increase, both presumably
221 because of biomass burning.

222
223 To put the 2020/2019 difference maps in a longer-term and seasonal context, [Figure 3](#)[Figure 3](#) shows monthly
224 averages of the four retrieved quantities over central east China since 2005. There are seasonal CO peaks in
225 March-April, June and September, with the minima usually in November and December ([Figure 3](#)[Figure 3](#)a).
226 There has been a decrease since 2005 in CO. The seasonal decrease from January to February in 2020 is similar
227 to that which has occurred occasionally before, but the CO during February and March 2020 was the lowest for
228 that time of the year since 2005. By April, CO had returned to levels typical of 2015-2019. The main
229 characteristics of the monthly SO₂ over the region are that it has decreased since 2005 ([Figure 3](#)[Figure 3](#)b), and
230 that early 2020 SO₂ was within the range of recent levels. There is a strong seasonal NO₂ cycle ([Figure 3](#)[Figure
231 3](#)c), with a July-August minimum, and December-January peak, which has been attributed to increased heating
232 needs (Yu et al., 2017;Si et al., 2019) and longer chemical lifetime owing to lower OH and RO₂ (Shah et al.,

233 2020). NO₂ has also decreased since 2011, and during most years, there is a departure from a smooth seasonal
234 cycle in January and February associated with the Chinese New Year holiday period. January and February 2020
235 NO₂ was considerably lower than previous years, increased during March, and had recovered to typical, recent
236 levels by April. AOD has consistent seasonal peaks in summer which have been attributed to hygroscopic growth
237 and agricultural residue burning (Filonchyk et al., 2019), but had less regular seasonality otherwise, and has
238 decreased since 2011. AOD during February and particularly March of 2020 were lower than recent years, but
239 during which time there was considerable variability in the monthly data.

240

241 [Figure 4](#)[Figure 4](#) shows the four retrieved quantities over southern China. There is a springtime maximum in CO
242 (Fig. 4a), a less regular maximum during September-January, and an annual minimum in July. The range of CO
243 is similar to central east China. CO over the last 5 years is lower than earlier in the record, and early 2020 CO was
244 higher than recent years. SO₂ (Fig. 4b) is lower than central east China and any seasonal cycle is also hard to
245 identify. The high June 2011 values are due to the Nabro eruption in Ethiopia (Fromm et al., 2014) which is still
246 apparent in the time series despite excluding individual SO₂ retrievals that are greater than 15 DU, and are due to
247 a combination of higher overall background values and individual retrievals with very high (> 10 DU) SO₂. NO₂
248 (Fig. 4c) is lower than over east central China, but both regions share a similar seasonality. NO₂ during January-
249 April 2020 was slightly lower than in 2019. AOD (Fig. 4d) has weak seasonal peaks in October, March and June,
250 has decreased since 2011, and 2020 fell within the range of 2015-2019.

251

252 3.2 East central China

253 Figure 5 shows the CO, SO₂, NO₂ and AOD for January 23 – April 8 of each year over east central China as box
254 and whisper plots with the median, interquartile range and 2.5th and 97.5th percentiles over all daily mean data as
255 horizontal lines and the mean shown by the black dot. The associated statistics comparing 2020 and 2019 are
256 provided in Table 1, ~~and comparing 2020 with the period over which the trend is most consistent in Table 2. which
257 was determined from the r^2 of the trends for all starting years between 2005 and 2016. The linear trends in each
258 plot start at the year over which the trend explains most of the variability in the data, which will vary by region
259 and variable, and comparing 2020 to longer background periods with and without trends accounted for as
260 supplementary Tables S1-S4.~~ The AIRS CO is shown in Figure 5a. The variation during January 23 – April 8 of
261 each year is due to weather-related factors and observational error. The mean CO of 133.5 ppbv in 2020 was 3.2%
262 less than the 2019 mean of 137.9 ppbv, ~~and 12% less than 2005-2019 mean of 150.9 ppbv. The 2020 difference
263 from 2019 is only which was only~~ marginally significant, ~~with having~~ with a 95% confidence interval (-6.3% - 0.1%)
264 close to spanning 0. ~~During years prior, there were increases and decreases in CO from year to year, but an overall
265 decreasing trend since 2005. To quantify if the 2020 departure was significant against this background, we
266 compared the distribution of observed 2020 CO to the background average and to that which might be expected
267 given any trends over the background period. Because there was no obvious starting year for the background
268 period, we considered different periods starting in each year between 2005 and 2018 and ending in 2019 (Fig. 6a,
269 Table S1). The difference between 2020 and the background depended strongly on the starting year of the
270 background period, ranging from -11.5% lower than the 2005-2019 mean to -3.1% lower than over 2018-2019,
271 but all were statistically significant. Significant trends over years beginning between 2005 and 2018 (shown in~~

272 Fig. 6a by the red line and shading) ranged between $-1.5 \text{ ppbv yr}^{-1}$ when starting in 2013 to $-3.6 \text{ ppbv yr}^{-1}$ if starting
273 in 2016. The uncertainty in the trends increased for trends over shorter periods, and were, unsurprisingly,
274 insignificant by 2017, with the 95% confidence intervals of the trends spanning 0. Figure 6 shows how the trends
275 and differences between observed and predicted 2020 means depended on the year chosen as the start of the period
276 over which the trend is estimated, for starting years between 2005 and 2016. AIRS CO (Fig. 6a) showed uneven
277 changes in the trend (red line) with starting year, and more uncertainty in the trend (red shading) for later years
278 due to fewer data used for the estimate, but for all years was significantly negative. The differences between the
279 observed 2020 mean and the value predicted from the trend (magenta line) varied inversely with the trend and
280 was always negative, but, except for 2009, had 95% confidence intervals (magenta shading) spanning 0, and
281 therefore were not considered significant. For CO therefore, 2020 was significantly lower than the background
282 period mean but not consistently lower than predicted given the decreasing trend during the background period,
283 no matter how this period was defined. The 2020 difference from the 2005-2019 background is significant (14%
284 -9%), but during this period CO declined by $-1.8 \text{ ppbv yr}^{-1}$, indicated by the red points. This overall decrease
285 includes periods where CO may have increased, for example from 2010-2012, 2016 and slightly in 2019. Based
286 on this trend, the expected value for 2020 was 136.8 ppbv (shown in blue). The observed 2020 mean was 2% less
287 than expected, but because the 95% confidence intervals (-5% -1%) span 0, this difference is not considered to
288 be significant. Results were similar for CO analysed closer to the surface at 850 hPa (not shown), but where the
289 retrieval has less sensitivity.

290

291 OMI SO₂ (Fig. 5b) fluctuated over 2005 to 2011 and declined steadily afterward ~~by $-0.056 \text{ DU yr}^{-1}$ from 2012-2019~~ over east central China. This trend explained 32% of the variation in the data over this period, during which overall variation also declined, becoming narrower to a degree not seen in the CO. Declines were steady, although 2019 may have departed upward from this trend. The 2020 mean of 0.058 ± 0.057 was 9495% higher than the 2019 mean of 0.031, but with a wide 95% confidence interval ($+1615\%$ -226250%). For different background periods (Table S2), 2020 SO₂ ranged from 83% less than the 2005-2019 mean to 30% less than the 2016-2019 mean, with insignificant differences compared to more recent periods. Trends varied significantly from -0.03 yr^{-1} over 2005-2019 to -0.06 DU yr^{-1} over 2012-2019 (Fig. 6b), during which the trend could explain a maximum of 32% of the variation in the data. For periods starting in 2007 and after, the observed 2020 mean was significantly higher than predicted. Relative to the value predicted from the 2012-2019 trend of -0.06 , the observed 2020 SO₂ was 2002% higher than the expected value of -0.06 ; the large percent difference reflects an expected predicted value close to zero, and we note that the retrieved SO₂ can be negative for individual values and averages (Li et al., 2013; Wang and Wang 2020). 2020 SO₂ was 72% lower than the 2012-2019 mean, and with a narrower (79% -65%) confidence interval. The observed 2020 SO₂ was 202% higher than the expected value of -0.06 ; the large percent difference reflects an expected value close to zero, and we note that the retrieved SO₂ can be negative for individual values and averages (Li et al., 2013; Wang and Wang 2020). While this difference was significant, the change in 2020 SO₂ was strongly dependent on whether daily values were calculated from the mean or median of individual values over the region. For most background periods (Figure S1b), the trends in the median values were still negative until 2015, but When the median of individual retrievals is used, 2020 was only 8.4% higher than predicted from the 2012-2019 trend and not significantly different from expected for trends beginning later.

311 (Figure S1b). This likely reflects the greater influence of high individual retrieval values on the daily mean value
312 compared to the median, even after the basic filtering of transient SO₂ plumes.

313 The SO₂ trends (Fig. 6b) were all significantly negative. For trends starting in 2007 and after, the observed 2020
314 mean was significantly higher than predicted, but these differences were not consistently significant when daily
315 values were calculated from the median of individual retrievals (Figure S2b).

316
317 OMI NO₂ (Fig. 5c) increased from 2005 to 2011 and decreased by 0.7×10^{15} molec cm⁻² yr⁻¹ from 2011
318 thereafter with an apparent flattening since 2016. The 2020 mean NO₂ of 6.5×10^{15} molec cm⁻² was 32% less
319 than the 2019 mean of 9.6×10^{15} molec cm⁻², and 43% less than the 2011-2019 mean of 11.3×10^{15} molec cm⁻². The
320 pronounced regional difference between 2020 and 2019 (Fig. 2c) in part likely reflects an upward departure
321 in 2019 from the overall trend since 2011 a 2019 uptick from 2018. For different background periods (Table S3),
322 2020 NO₂ ranged from 43.3% less than the 2010-2019 mean to 30% less than the 2018-2019 mean, with all
323 differences significant. Trends were negative and significant for starting years between 2007 and 2015 (Fig. 6c)
324 with the strongest trend of -0.75×10^{15} molec cm⁻² yr⁻¹ for the period beginning in 2011. 2020 NO₂ was
325 significantly less than the predicted value for all background periods but varied from 16.8% less than predicted
326 from the 2011-2019 trend to 27.1% less than predicted from the 2015-2019 trend, the last period when there was
327 a significant, although weak, decrease.

328
329 The observed 2020 mean was 17% less than the expected value of 7.8×10^{15} molec cm⁻², with a wide but negative
330 95% confidence interval (-28% -5%), suggesting that 2020 NO₂ was significantly lower than would be expected
331 from the trend.

332 Earlier starting years produce weaker overall trends in NO₂ (Fig. 6c) because of the NO₂ increase until 2011, but
333 observed 2020 NO₂ was significantly less than predicted regardless of the starting year. As the NO₂ trend
334 approached 0 for periods beginning after 2012, the 2020 differences from what would be expected increased. For
335 a period beginning in 2016, for example, the 2020 NO₂ was 32.8% less than the mean over this period and 28.9%
336 less than what would be expected from the trend. Note that analyses of SO₂ and NO₂ that include years prior to
337 2012 may be affected by changes in observation sample size due to changes in the OMI row anomaly.

338 MODIS AOD (Fig. 5d) was flat or slightly increasing from 2005 to 2011, decreasing thereafter and with a
339 flattening since 2016 similar to SO₂ and NO₂, and subsequently changed by 0.03 yr^{-1} . The 2020 mean AOD of
340 0.41 was 14% less than the 2019 mean of 0.48, but this was not significant and 29% less than the 2011-2019
341 average of 0.58. For different background periods (Table S4), 2020 AOD ranged from 30.2% less than the 2007-
342 2019 mean to 14.2% less than the 2018-2019 mean, confidence intervals for the differences becoming closer to
343 spanning 0 for more recent periods. Trends were negative and significant for starting years between 2005 and
344 2014 (Fig. 6d), with the strongest decrease of 0.04 yr^{-1} over the 2012-2019 period. The observed 2020 mean was
345 2% higher than the predicted value of 0.40, but with a wide (-15% -20%) confidence interval spanning 0,
346 suggesting 2020 was not significantly different from expected.

347
348 In evaluating the 2020 changes, the background period was defined by the period during which the trend was
349 strongest, using the r^2 value of the trend. This is a reasonable but ad hoc way of defining a period with consistent
350 increasing or decreasing trends. Figure 6 shows how the trends and differences between observed and predicted

351 ~~2020 means depended on the year chosen as the start of the period over which the trend is estimated, for starting~~
352 ~~years between 2005 and 2016. AIRS CO (Fig. 6a) showed uneven changes in the trend (red line) with starting~~
353 ~~year, and more uncertainty in the trend (red shading) for later years due to fewer data used for the estimate, but~~
354 ~~for all years was significantly negative. The difference between observed 2020 mean and the value predicted from~~
355 ~~the trend (magenta line) varied inversely with the trend and was always negative, but, except for 2009, had 95%~~
356 ~~confidence intervals (magenta shading) spanning 0, and therefore were not considered significant. The SO₂ trends~~
357 ~~(Fig. 6b) were all significantly negative. For trends starting in 2007 and after, the observed 2020 mean was~~
358 ~~significantly higher than predicted, but these differences were not consistently significant when daily values were~~
359 ~~calculated from the median of individual retrievals (Figure S2b). Earlier starting years produce weaker overall~~
360 ~~trends in NO₂ (Fig. 6c) because of the NO₂ increase until 2011, but observed 2020 NO₂ was significantly less than~~
361 ~~predicted regardless of the starting year. As the NO₂ trend approached 0 for periods beginning after 2012, the~~
362 ~~2020 differences from what would be expected increased. For a period beginning in 2016, for example, the 2020~~
363 ~~NO₂ was 32.8% less than the mean over this period and 28.9% less than what would be expected from the trend.~~
364 ~~Note that analyses of SO₂ and NO₂ that include years prior to 2012 may be affected by changes in observation~~
365 ~~sample size due to changes in the OMI raw anomaly. For AOD (Fig. 6d), there was no significant difference~~
366 ~~between the observed and predicted 2020 mean for periods beginning in 2009–2008 and later, when the trends~~
367 ~~were strongest, and which approached 0 after 2014.~~

368 3.3 Southern China

369 Figure 7 shows the distribution of daily CO, SO₂, NO₂ and AOD for January 23–April 8 of each year over southern
370 China, ~~along with linear trends~~. The associated statistics comparing 2020 and 2019 are provided in ~~Table 2~~
371 ~~Table 3, and comparing 2020 with the period over which the trend is consistent in Table 4. For~~ AIRS CO (Fig. 7a) ~~in~~
372 ~~a~~ in 2020 was 144.9 ~~7~~ ppbv, 13% higher than the 2019 mean of 128.4 ~~5~~ ppbv which can be seen in an upward shift
373 in the distribution of the box plot, and higher than the 2016–2019 background period mean of 137 ppbv. ~~2020~~
374 ~~2020 CO was 16% higher than predicted from the 2016–2019 trend, and with 95% confidence interval (10%–~~
375 ~~23%) not spanning 0. CO was between 4.4% and 8.8% greater than the background mean for periods starting after~~
376 ~~2014 (Table S5), but not significantly different otherwise. CO decreased significantly for periods starting between~~
377 ~~2005 and 2016 (Fig. 8a). When these trends are taken into account, 2020 CO was between 11.2% and 18.7%~~
378 ~~greater than predicted, and in all cases were significant.~~

379
380 OMI SO₂ (Fig. 7b) ~~changed by -0.012 DU yr⁻¹ beginning in 2007, fluctuated from 2005 until 2013 and flattened~~
381 ~~afterwards, which is driven by fewer high individual SO₂ values in later years, as in east central China. The 2020~~
382 mean of 0.003 DU was ~~122.116~~ % higher than the 2019 mean of -0.023 DU ~~but also~~ with a wide ~~but positive~~ 95%
383 confidence interval (~~20.24% - 21.723%~~), and 95% less than the 2007–2019 mean of 0.058 DU. ~~2020 was less~~
384 ~~than the background mean for periods starting between 2005 and 2011 (Table S6), but not significantly different~~
385 ~~otherwise. SO₂ trends were consistently negative for all periods (Fig. 8b), although not as strong as over east~~
386 ~~central China. SO₂ trends were also negative, and varied similarly to the CO until 2015. The observed 2020 mean~~
387 ~~was 109% higher than the predicted value of -0.034 DU, with a wide but positive 95% confidence interval (53%–~~
388 ~~165%). Whether 2020 SO₂ was greater than predicted from trends depended more on the background period than~~

389 over east central China and were also not significantly different from predicted when daily values were calculated
390 from the median SO₂ of individual retrievals for any background period (Figure S2b).

391
392 OMI NO₂ (Fig. 7c) increased toward 2011 and 2012, declining after to 2005-2010 levels. changed by 0.3×10^{15}
393 molec cm⁻² yr⁻¹ beginning in 2011. The 2020 mean of 3.3×10^{15} molec cm⁻² was 22% less than the 2019 mean of
394 4.3×10^{15} molec cm⁻² and 32% less than 2011-2019, with both differences significant. For longer background
395 periods, 2020 was between 22.9% and 30.6% less than the mean (Table S7), all of which were significant. NO₂
396 trends were significantly negative for periods beginning between 2007 and 2012, but not otherwise (Fig. 8c). The
397 2020 mean was 7% less than the predicted value of 3.6×10^{15} molec cm⁻², but with a wide 95% confidence interval
398 (-19% - 8%) spanning 0. NO₂ trends (Fig. 8c) were more strongly decreasing for periods beginning between 2009
399 and 2012 and were flat or positive otherwise. The 2020 NO₂ mean was significantly lower than predicted, except
400 for when the trend was estimated beginning in 2011, when it was the strongest, or 2018. A two-year trend is hard
401 to interpret meaningfully, but visually, it is hard to tell if the 2020 NO₂ distribution represents a COVID-related
402 departure or a decrease comparable to changes during recent previous years, unlike over central east China.
403

404 MODIS AOD (Fig. 7d) changed by 0.04 yr^{-1} between 2011 and 2019 was comparable to NO₂ in its increase
405 toward 2012, decrease thereafter and flattening during more recent years. The 2020 mean AOD of 0.38 was 12%
406 higher than the 2019 mean of 0.34, but with a 95% confidence interval (-67% - 323%) spanning 0. Similarly,
407 2020 was between 14% and 22% lower than during background periods beginning from 2005 to 2012, but not for
408 more recent periods (Table S8). 2020 AOD was 17% less than the 2011-2019 mean of 0.46, but 39% higher than
409 predicted from the trend over this period, and with a wide but positive 95% confidence interval (15% - 68%).
410

411 Figure 8 shows the dependence of the trends and 2020 differences from background period to the starting year
412 over southern China. AIRS CO (Fig. 8a) had a significant decreasing trend for all starting years, and regardless
413 of the start year, 2020 was significantly higher than predicted from the trend. SO₂ trends were also negative, and
414 varied similarly to the CO until 2015. The 2020 SO₂ was higher than the background period, but with marginal
415 significance, given that the confidence intervals spanned 0 for later starting years, and because the differences
416 were not significant when daily values were calculated from the median SO₂ of individual retrievals for trends
417 starting in 2008 (Figure S3b) or any other year (Figure S4b). NO₂ trends (Fig. 8c) were more strongly decreasing
418 for periods beginning between 2009 and 2012 and were flat or positive otherwise. The 2020 NO₂ mean was
419 significantly lower than predicted, except for when the trend was estimated beginning in 2011, when it was the
420 strongest. The AOD trends varied similarly to the NO₂ but were significantly negative for all start years until
421 2015. The 2020 mean was significantly higher between 32 and 47% higher than predicted from trends for periods
422 starting for all starting between 2010 and 2015, but not otherwise.

423
424 For both regions and all quantities, the differences between observed and predicted values for 2020 were
425 insensitive to a longer lockdown period, or to whether the bootstrap resampling was weighted by the number of
426 valid retrievals each day. For a February-only lockdown period (Figures S5 and S6), the CO trends were more
427 significant when starting in later years, but the differences between the observed and expected values for remained
428 insignificant. The SO₂ trends for different periods were similar. The 2020 SO₂ differences from what would be

429 expected approached 0 for later periods but were also in inconsistent when the median values of individual
430 retrievals were used. Results for NO₂ were unaffected. The AOD 2020 difference from what would be expected
431 was stronger and technically significant, but still with a very wide confidence interval and therefore difficult to
432 interpret. We emphasize that while a February-only lockdown period is useful for comparison, it is problematic
433 in not including the New Year's holiday periods from all previous years.

434 **4 Discussion and conclusions**

435 The degree to which the COVID-19 lockdowns in China resulted in changes in atmospheric composition ~~depends~~
436 ~~depended~~ strongly on ~~the background period and~~ whether existing trends ~~are-were~~ taken into account. ~~and only in~~
437 ~~certain cases could be considered significant~~. For AIRS CO over central east China, the 2020 mean was 12% less
438 than that over 2005-2019 ~~and 3% lower than since 2018, but was not consistently different from, but only 2% less~~
439 ~~than~~ what would be expected given the steady decreases over ~~that different periods, and this 2% was not significant~~
440 ~~given the variability of the daily data.~~ Similarly for MODIS AOD, the 2020 mean was ~~between 14% and 30%~~
441 less than ~~over 2011-2019 different background averages~~, but not ~~significantly~~ different ~~than what would be from~~
442 ~~what would be expected from trends for trends beginning after 2008. SO₂ in 2020 was 72% less than over 2012-~~
443 ~~2019 but was 201% higher than what would be expected from trends. Daily SO₂ calculated from the mean of~~
444 ~~individual retrievals are sensitive to outlying SO₂ values from transient plumes, and when daily SO₂ was calculated~~
445 ~~instead from the median across individual retrievals, 2020 SO₂ was only 8% higher than what would be expected,~~
446 ~~but still significantly. 2020 SO₂ was significantly lower than background averages calculated over most periods,~~
447 ~~ranging from 83% less than over 2005-2019 to 30% less than over 2016-2019. Compared to the 2012-2019 period~~
448 ~~when there were no significant SO₂ increases, 2020 SO₂ was 200% greater than what would be expected, but only~~
449 ~~8% greater when the median value was used, and not significantly different from expected relative to the trends~~
450 ~~beginning later than 2012. We Earlier starting years produce weaker overall trends in NO₂ (Fig. 6e) because of~~
451 ~~the NO₂ increase until 2011, but observed 2020 NO₂ was significantly less than predicted regardless of the starting~~
452 ~~year. As the NO₂ trend approached 0 for periods beginning after 2012, the 2020 differences from what would be~~
453 ~~expected increased. For a period beginning in 2016, for example, the 2020 NO₂ was 32.8% less than the mean~~
454 ~~over this period and 28.9% less than what would be expected from the trend. note that analyses of SO₂ and NO₂~~
455 ~~that include years prior to 2012 may be affected by changes in observation sample size due to changes in the OMI~~
456 ~~row anomaly.~~

457
458
459 OMI NO₂ in 2020 over central east China was ~~consistently lower than the background average and expected value~~
460 ~~from the trends, but the latter value ranged from 17% for a trend calculated over 2011-2019 to a 33% decrease~~
461 ~~compared to 2018-2019 during which NO₂ trends had flattened. 43% less than over 2011-2019, but only 17% less~~
462 ~~than what would be expected from trends. This difference was statistically significant. While there were clear~~
463 ~~decreases in 2020 NO₂, this but does suggest that more than half some part of the reductions in NO₂ in 2020 could~~
464 be expected independent of COVID-19 lockdowns. For reference, Bauwens et al. (2020) reported a ~40% drop in
465 OMI NO₂ from 2019 to 2020 over cities affected by the lockdown using the QA4ECV retrieval (Boersma et al.,
466 2018), and a ~51% drop in NO₂ over the eight cities (Beijing, Jinan, Nanjing, Qingdao, Tianjin, Wuhan, Xi'an
467 and Zhengzhou) falling within our central east China region. Our analysis cannot be compared directly because

468 we include non-urban areas and define ~~our the~~ lockdown period differently, but we can say that ~~a large part some~~
469 of the reduction in that study is ~~likely possibly~~ due to background trends, ~~rather than in addition~~ to COVID-19
470 lockdowns.

471
472 The lack of any significant departure from recent trends in CO and AOD over central east China was unexpected,
473 given its high population density and level of industrial activity. In the case of MODIS AOD, the lack of an
474 observable lockdown effect was possibly due to contributions from other sources unaffected by COVID-19 related
475 lockdowns, limitations in the MODIS AOD retrieval under cloudy conditions, climatological variability from
476 other sources such as mineral dust, and meteorology favourable to secondary aerosol formation which could have
477 offset lower emissions (Wang et al., 2020). The 2020 increase in SO₂ is more difficult to interpret because of the
478 discrepancies between daily values calculated from the mean or median of individual retrievals, but is broadly
479 consistent with surface observations that find no significant change in in-situ surface SO₂ over Wuhan in the daily
480 mean, and a slight increase in daytime SO₂ possibly associated with increased residential heating and cooking
481 (Shi and Brasseur, 2020).

482
483 Over southern China, retrieved ~~2020 SO₂ was significantly lower than the background average only for periods~~
484 ~~beginning between 2005 to 2011. Significant departures from expected trends uneven for the mean value and~~
485 ~~absent for the median value. NO₂ and AOD were significantly lower in 2020 compared to recent averages. SO₂~~
486 ~~was 95% less than the 2007 2019 mean, but 109% greater than what would be expected from trends. Similarly to~~
487 ~~central east China, SO₂ was only 5% higher than expected when daily values were calculated from the median of~~
488 ~~individual retrievals, rather than the mean. NO₂ in 2020 was between 23% and 32% less than the background~~
489 ~~average for over 2011 2019 different periods, but only 7% less than what would be expected from trends, and this~~
490 ~~difference was not consistently significant for different trend periods and between 14% and 23% less than expected~~
491 ~~from trends, with insignificant differences when trends were calculated beginning in 2011 or 2018.~~ The more
492 significant reductions in NO₂ in east central China compared to the south is presumably due the former's greater
493 population and industrialization, and consequently higher pollution levels. This is consistent with Chen et al.'s
494 (2020) detection of a larger 2020 decrease in surface NO₂ in Wuhan compared to Shanghai. Retrieved CO in 2020
495 was ~~nearly identical to the 2007 2019 mean between 4 and 8% greater than background averages beginning in~~
496 ~~2014, but 10 between 11% and 19% higher than what would be expected given the decreasing trends over this any~~
497 period. AOD in 2020 was ~~lower than background averages beginning until 2012 17% less than over 2011 2019,~~
498 ~~but higher or not significantly different from expected for trends beginning after 39% higher than what would be~~
499 ~~expected from the trend.~~

500
501 The focus of this analysis is on whether satellite retrievals of atmospheric composition over 2020 departed
502 significantly from different background periods and expected values for 2020 when daily variability and trends
503 are accounted for, but it is useful at a preliminary stage to speculate as to how different emissions changes could
504 have contributed to 1) why NO₂ was robustly lower in 2020 over east central China compared to CO and AOD,
505 and 2) why CO and ~~perhaps~~ AOD were higher over southern China compared to what would be expected from
506 recent trends.

508 To understand why NO₂ differences over east central China were more significant than other quantities, [Table 3](#)
509 [Table 5](#) shows the emissions by sector for a representative set of constituents from the Community Emissions
510 Data System (CEDS) (Hoesly et al., 2018) over China for 2014, the most recent year available. Other bottom-up
511 emissions inventories will vary in absolute emissions amounts and their sector contributions, particularly for more
512 recent periods, but CEDS is the standard available emissions dataset available globally as a baseline for the next
513 IPCC assessment, in anticipation of assessing 2020 COVID-19 related changes to atmospheric composition in
514 other regions, and for modeling studies involving a transboundary transport component. Across all species, energy
515 production, industrial activity, transportation, residential/commercial/other (RCO), and waste disposal constitute
516 the bulk of the emissions. Based on activity data for the first quarter of 2020, energy demand across China declined
517 by 7% compared to 2019, and transportation sector activity declined by 50 to 75% in regions with lockdowns in
518 place (International Energy Agency, 2020). These sectors are direct or indirect sources of numerous pollutants,
519 including SO₂ (the precursor of sulfate aerosol), NO_x, CO, and primary anthropogenic aerosols classified broadly
520 as organic carbon (OC) and black carbon (BC). If we apply the 7% reduction in energy production and mid-point
521 62.5% reduction to transportation from the IEA, assume a 20% reduction in industrial emissions, 5% reduction in
522 waste emissions, no change in RCO (with commercial decreases offset by residential increases), this yields a 10%
523 reduction in BC, 5% reduction in OC, 14% reduction in SO₂, 14% reduction in CO and 21% reduction in NO₂.
524 The larger reduction in NO₂ relative to other emissions could partly explain why OMI NO₂ column density
525 changes over central east China were stronger than in the other retrievals.

526
527 Following Si et al.'s (2019) consideration of biomass burning as a pollution source in China alongside
528 anthropogenic sources, we considered transboundary smoke transport as a possible reason for the higher 2020 CO
529 over southern China, guided by higher CO over the Upper Mekong region in 2020 compared to 2019 (Fig. 2a)
530 and the predominant westerly flow during this time of year (Reid et al., 2013). [Table 4](#)[Table 6](#) compares January
531 23-April 8 AIRS CO over southern China to CO emissions estimates from biomass burning from the Global Fire
532 Assimilation System (GFAS) (Kaiser et al., 2012) over the upper Mekong region (17° N to 25° N, 95° E to 105°
533 E) including parts of eastern Myanmar, northern Thailand, and northern Laos. From 2005 to 2020, variation in
534 GFAS CO over this region explained a moderate (32%) amount of variability in AIRS CO over southern China,
535 suggesting it as a non-negligible contributor to variation in CO concentration, and a contributor to higher CO
536 in 2020. This illustrates that, at a minimum, sources such as biomass burning smoke and dust that are less affected
537 by COVID-19 related measures will complicate attribution studies. To that end, modeling studies following Wang
538 et al. (2020) will be required to isolate emissions, meteorological and chemical drivers of changes in atmospheric
539 composition and their effects at a process level. With proper instrument-equivalent comparisons, modelling
540 studies will also help to identify the extent to which the lack of significant changes are due to retrieval limitations,
541 namely low sensitivity near the surface where differences would presumably be more pronounced, particularly
542 given remote emissions sources such as dust, biomass burning smoke and volcanic SO₂, which will arrive at higher
543 altitudes.

544
545 The key implication of our study is that [interpreting differences in 2020 retrievals of atmospheric composition](#)
546 [depends strongly on how the background period is defined and whether trends over these periods are accounted](#)
547 [for. Not taking into account taking these into account past trends in atmospheric composition will could lead](#)

548 to misattribution of changes in air quality to COVID-19 lockdowns, or, at a minimum, that whether differences
549 in 2020 are significant depend on the choice of ~~detrending period and lockdown periods~~^{background period}, given
550 ~~its~~^{which is somewhat} subjective~~ivity~~. We have approached the issue by comparing data for 2020 to what would
551 have been expected given recent trends and by applying a single lockdown period to two large regions, with
552 additional analyses to gauge the sensitivity of the 2020 differences to these choices. Other studies over China or
553 elsewhere will inevitably use other approaches that more explicitly account for seasonality, meteorology, and
554 which relate changes in pollution over smaller areas (e.g. single provinces or states) to region-specific lockdown
555 measures and timing at a process level. Regardless of the approach, however, it is important to consider recent
556 trends and variability. In places where pollution has decreased, not accounting for recent context ~~will~~^{could} result
557 in over-attribution of changes in pollution to COVID-19. In places where pollution has increased, such as parts of
558 South Asia, this ~~will~~^{could} result in under-attribution.

559 **Code/data availability:** All code will be made available if the article is accepted for final publication. All source
560 data are publicly available.

561

562 **Competing interests:** The authors have no competing interests.

563

564 **Author contribution:** All authors conceived of the study. RF, IG and KT conducted the data analysis. RF and
565 JH prepared the manuscript with contributions from all co-authors.

566

567

References

568 Bauwens, M., Compernolle, S., Stavrakou, T., Müller, J., van Gent, J., Eskes, H., Levelt, P. F., van der A., R.,
 569 Veefkind, J. P., Vlietinck., J., Yu, H., and Zehner, C.: Impact of coronavirus outbreak on NO₂ pollution assessed using
 570 TROPOMI and OMI observations, *Geophysical Research Letters*, 2, 0-3, 10.1029/2020GL087978, 2020.

571 Boersma, K. F., Eskes, H. J., Richter, A., De Smedt, I., Lorente, A., Beirle, S., van Geffen, J., Zara, M., Peters, E.,
 572 Van Roozendael, M., Wagner, T., Maasakkers, J. D., van der A, R. J., Nightingale, J., De Rudder, A., Irie, H., Pinardi,
 573 G., Lambert, J. C., and Compernolle, S. C.: Improving algorithms and uncertainty estimates for satellite NO₂
 574 retrievals: results from the quality assurance for the essential climate variables (QA4ECV) project, *Atmospheric*
 575 *Measurement Techniques*, 11, 6651-6678, 10.5194/amt-11-6651-2018, 2018.

576 Castellanos, P., Boersma, K. F., Torres, O., and de Haan, J. F.: OMI tropospheric NO₂ air mass factors over South
 577 America: effects of biomass burning aerosols, *Atmospheric Measurement Techniques*, 8, 3831-3849, 10.5194/amt-8-
 578 3831-2015, 2015.

579 Chen, K., Wang, M., Huang, C., Kinney, P. L., and Paul, A. T.: Air Pollution Reduction and Mortality Benefit during
 580 the COVID-19 Outbreak in China, *Lancet Planetary Health*, 0-3, 10.1101/2020.03.23.20039842, 2020.

581 Chimot, J., Vleminck, T., Veefkind, J. P., de Haan, J. F., and Levelt, P. F.: Impact of aerosols on the OMI tropospheric
 582 NO₂ retrievals over industrialized regions: how accurate is the aerosol correction of cloud-free scenes via a simple
 583 cloud model?, *Atmospheric Measurement Techniques*, 9, 359-382, 10.5194/amt-9-359-2016, 2016.

584 Efron, B., and Gong, G.: A Leisurely Look at the Bootstrap, the Jackknife, and Cross-Validation, *American Statistician*,
 585 37, 36-48, 10.2307/2685844, 1983.

586 Filonchyk, M., Yan, H. W., and Zhang, Z. R.: Analysis of spatial and temporal variability of aerosol optical depth
 587 over China using MODIS combined Dark Target and Deep Blue product, *Theoretical and Applied Climatology*, 137,
 588 2271-2288, 10.1007/s00704-018-2737-5, 2019.

589 Fioletov, V. E., McLinden, C. A., Krotkov, N., Li, C., Joiner, J., Theys, N., Carn, S., and Moran, M. D.: A global
 590 catalogue of large SO₂ sources and emissions derived from the Ozone Monitoring Instrument, *Atmospheric Chemistry*
 591 and Physics, 16, 11497-11519, 10.5194/acp-16-11497-2016, 2016.

592 Fromm, M., Kablick, G., Nedoluha, G., Carboni, E., Grainger, R., Campbell, J., and Lewis, J.: Correcting the record
 593 of volcanic stratospheric aerosol impact: Nabro and Sarychev Peak, *Journal of Geophysical Research-Atmospheres*,
 594 119, 10.1002/2014jd021507, 2014.

595 Geddes, J. A., Martin, R. V., Boys, B. L., and van Donkelaar, A.: Long-Term Trends Worldwide in Ambient NO₂
 596 Concentrations Inferred from Satellite Observations, *Environmental Health Perspectives*, 124, 281-289,
 597 10.1289/ehp.1409567, 2016.

598 Georgoulias, A. K., van der A, R. J., Stammes, P., Boersma, K. F., & Eskes, H. J.: Trends and trend reversal detection
 599 in two decades of tropospheric NO₂ satellite observations, *Atmospheric Chemistry and Physics*, 19, 6269–6294,
 600 <https://doi.org/10.5194/acp-2018-988>, 2019.

601 Han, H., Liu, J., Yuan, H. L., Jiang, F., Zhu, Y., Wu, Y., Wang, T. J., and Zhuang, B. L.: Impacts of Synoptic Weather
 602 Patterns and their Persistency on Free Tropospheric Carbon Monoxide Concentrations and Outflow in Eastern China,
 603 *Journal of Geophysical Research-Atmospheres*, 123, 7024-7046, 10.1029/2017jd028172, 2018.

604 He, Q. Q., Gu, Y. F., and Zhang, M.: Spatiotemporal patterns of aerosol optical depth throughout China from 2003 to
605 2016, *Science of the Total Environment*, 653, 23-35, 10.1016/j.scitotenv.2018.10.307, 2019.

606 Hoesly, R. M., Smith, S. J., Feng, L. Y., Klimont, Z., Janssens-Maenhout, G., Pitkanen, T., Seibert, J. J., Vu, L.,
607 Andres, R. J., Bolt, R. M., Bond, T. C., Dawidowski, L., Kholod, N., Kurokawa, J., Li, M., Liu, L., Lu, Z. F., Moura,
608 M. C. P., O'Rourke, P. R., and Zhang, Q.: Historical (1750-2014) anthropogenic emissions of reactive gases and
609 aerosols from the Community Emissions Data System (CEDS), *Geoscientific Model Development*, 11, 369-408,
610 10.5194/gmd-11-369-2018, 2018.

611 Hubanks, P., Platnick, S., King, M., and Ridgway, B.: MODIS Algorithm Theoretical Basis Document No. ATBD-
612 MOD-30 for Level-3 Global Gridded Atmosphere Products (08_D3, 08_E3, 08_M3) and Users Guide (Collection 6.0
613 & 6.1, Version 4.4, 20 Feb 2019), NASA Goddard Space Flight Center, Greenbelt, MD, 2019.

614 Kaiser, J. W., Heil, A., Andreae, M. O., Benedetti, A., Chubarova, N., Jones, L., Morcrette, J. J., Razinger, M., Schultz,
615 M. G., Suttie, M., and van der Werf, G. R.: Biomass burning emissions estimated with a global fire assimilation system
616 based on observed fire radiative power, *Biogeosciences*, 9, 527-554, 10.5194/bg-9-527-2012, 2012.

617 Krotkov, N. A.: OMI/Aura NO₂ Cloud-Screened Total and Tropospheric Column L3 Global Gridded 0.25 degree x
618 0.25 degree V3, NASA Goddard Space Flight Center, 2013.

619 Krotkov, N. A., McLinden, C. A., Li, C., Lamsal, L. N., Celarier, E. A., Marchenko, S. V., Swartz, W. H., Bucsela,
620 E. J., Joiner, J., Duncan, B. N., Boersma, K. F., Veefkind, J. P., Levelt, P. F., Fioletov, V. E., Dickerson, R. R., He,
621 H., Lu, Z., and Streets, D. G.: Aura OMI observations of regional SO₂ and NO₂ pollution changes from 2005 to 2015,
622 *Atmospheric Chemistry and Physics*, 16, 4605-4629, 10.5194/acp-16-4605-2016, 2016.

623 Krotkov, N. A., Lamsal, L. N., Celarier, E. A., Swartz, W. H., Marchenko, S. V., Bucsela, E. J., Chan, K. L., Wenig,
624 M., and Zara, M.: The version 3 OMI NO₂ standard product, *Atmospheric Measurement Techniques*, 10, 3133-3149,
625 10.5194/amt-10-3133-2017, 2017.

626 Lamsal, L. N., Krotkov, N. A., Celarier, E. A., Swartz, W. H., Pickering, K. E., Bucsela, E. J., Gleason, J. F., Martin,
627 R. V., Philip, S., Irie, H., Cede, A., Herman, J., Weinheimer, A., Szykman, J. J., and Knepp, T. N.: Evaluation of OMI
628 operational standard NO₂ column retrievals using in situ and surface-based NO₂ observations, *Atmospheric
629 Chemistry and Physics*, 14, 11587-11609, 10.5194/acp-14-11587-2014, 2014.

630 Levy, R. C., Remer, L. A., Kleidman, R. G., Mattoo, S., Ichoku, C., Kahn, R., and Eck, T. F.: Global evaluation of
631 the Collection 5 MODIS dark-target aerosol products over land, *Atmospheric Chemistry and Physics*, 10, 10399-
632 10420, 10.5194/acp-10-10399-2010, 2010.

633 Li, C., Joiner, J., Krotkov, N. A., and Bhartia, P. K.: A fast and sensitive new satellite SO₂ retrieval algorithm based
634 on principal component analysis: Application to the ozone monitoring instrument, *Geophysical Research Letters*, 40,
635 6314-6318, 10.1002/2013gl058134, 2013.

636 Li, M., Zhang, Q., Kurokawa, J., Woo, J. H., He, K. B., Lu, Z. F., Ohara, T., Song, Y., Streets, D. G., Carmichael, G.
637 R., Cheng, Y. F., Hong, C. P., Huo, H., Jiang, X. J., Kang, S. C., Liu, F., Su, H., and Zheng, B.: MIX: a mosaic Asian
638 anthropogenic emission inventory under the international collaboration framework of the MICS-Asia and HTAP,
639 *Atmospheric Chemistry and Physics*, 17, 935-963, 10.5194/acp-17-935-2017, 2017.

640 Lin, C. Q., Liu, G., Lau, A. K. H., Li, Y., Li, C. C., Fung, J. C. H., and Lao, X. Q.: High-resolution satellite remote
641 sensing of provincial PM 2.5 trends in China from 2001 to 2015. *Atmospheric Environment*, 180, 110-116,
642 <https://doi.org/10.1016/j.atmosenv.2018.02.045>, 2018.

643 Lin, N., Wang, Y. X., Zhang, Y., and Yang, K.: A large decline of tropospheric NO₂ in China observed from space
644 by SNPP OMPS, *Science of the Total Environment*, 675, 337-342, 10.1016/j.scitotenv.2019.04.090, 2019.

645 Luan, Y., and Jaegle, L.: Composite study of aerosol export events from East Asia and North America, Atmospheric
646 Chemistry and Physics, 13, 1221-1242, 10.5194/acp-13-1221-2013, 2013.

647 Ma, Z. W., Hu, X. F., Sayer, A. M., Levy, R., Zhang, Q., Xue, Y. G., Tong, S. L., Bi, J., Huang, L., and Liu, Y.:
648 Satellite-Based Spatiotemporal Trends in PM2.5 Concentrations: China, 2004-2013, Environmental Health
649 Perspectives, 124, 184-192, 10.1289/ehp.1409481, 2016.

650 McLinden, C. A., Fioletov, V., Boersma, K. F., Kharol, S. K., Krotkov, N., Lamsal, L., Makar, P. A., Martin, R. V.,
651 Veefkind, J. P., and Yang, K.: Improved satellite retrievals of NO₂ and SO₂ over the Canadian oil sands and
652 comparisons with surface measurements, Atmospheric Chemistry and Physics, 14, 3637-3656, 10.5194/acp-14-3637-
653 2014, 2014.

654 Mijling, B., van der A, R. J., Boersma, K. F., Van Roozendael, M., De Smedt, I., and Kelder, H. M.: Reductions of
655 NO₂ detected from space during the 2008 Beijing Olympic Games, Geophysical Research Letters, 36,
656 10.1029/2009gl038943, 2009.

657 Reid, J. S., Hyer, E. J., Johnson, R. S., Holben, B. N., Yokelson, R. J., Zhang, J. L., Campbell, J. R., Christopher, S. A., Di
658 Girolamo, L., Giglio, L., Holz, R. E., Kearney, C., Miettinen, J., Reid, E. A., Turk, F. J., Wang, J., Xian, P., Zhao, G. Y.,
659 Balasubramanian, R., Chew, B. N., Janjai, S., Lagrosas, N., Lestari, P., Lin, N. H., Mahmud, M., Nguyen, A. X., Norris, B.,
660 Oanh, N. T. K., Oo, M., Salinas, S. V., Welton, E. J., and Liew, S. C.: Observing and understanding the Southeast Asian
661 aerosol system by remote sensing: An initial review and analysis for the Seven Southeast Asian Studies (7SEAS) program,
662 Atmospheric Research, 122, 403-468, 10.1016/j.atmosres.2012.06.005, 2013.

663 Sarkodie, S. A., and Strezov, V.: A review on Environmental Kuznets Curve hypothesis using bibliometric and meta-
664 analysis, Science of the Total Environment, 649, 128-145, 10.1016/j.scitotenv.2018.08.276, 2019.

666 Sayer, A. M., Hsu, N. C., Bettenhausen, C., and Jeong, M. J.: Validation and uncertainty estimates for MODIS
667 Collection 6 "Deep Blue" aerosol data, Journal of Geophysical Research-Atmospheres, 118, 7864-7872,
668 10.1002/jgrd.50600, 2013.

669 Sayer, A. M., Munchak, L. A., Hsu, N. C., Levy, R. C., Bettenhausen, C., and Jeong, M. J.: MODIS Collection 6
670 aerosol products: Comparison between Aqua's e-Deep Blue, Dark Target, and "merged" data sets, and usage
671 recommendations, Journal of Geophysical Research-Atmospheres, 119, 13965-13989, 10.1002/2014jd022453, 2014.

672 Schutgens, N., Sayer, A. M., Heckel, A., Hsu, C., Jethva, H., de Leeuw, G., Leonard, P. J. T., Levy, R. C., Lipponen,
673 A., Lyapustin, A., North, P., Popp, T., Poulson, C., Sawyer, V., Sogacheva, L., Thomas, G., Torres, O., Wang, Y.,
674 Kinne, S., Schulz, M., and Stier, P.: An AeroCom/AeroSat study: Intercomparison of Satellite AOD Datasets for
675 Aerosol Model Evaluation, Atmos. Chem. Phys. Discuss., 2020, 1-43, 10.5194/acp-2019-1193, 2020.

676 Selden, T. M., and Song, D. Q.: Environmental Quality and Development - is there a Kuznets Curve for Air-Pollution
677 Emissions?, Journal of Environmental Economics and Management, 27, 147-162, 10.1006/jeem.1994.1031, 1994.

678 Shah, V., Jacob, D. J., Li, K., Silvern, R. F., Zhai, S. X., Liu, M. Y., Lin, J. T., and Zhang, Q.: Effect of changing NO_x
679 lifetime on the seasonality and long-term trends of satellite-observed tropospheric NO₂ columns over China,
680 Atmospheric Chemistry and Physics, 20, 1483-1495, 10.5194/acp-20-1483-2020, 2020.

681 Shao, P. Y., Tian, H. Z., Sun, Y. J., Liu, H. J., Wu, B. B., Liu, S. H., Liu, X. Y., Wu, Y. M., Liang, W. Z., Wang, Y.,
682 Gao, J. J., Xue, Y. F., Bai, X. X., Liu, W., Lin, S. M., and Hu, G. Z.: Characterizing remarkable changes of severe
683 haze events and chemical compositions in multi-size airborne particles (PM₁, PM_{2.5} and PM₁₀) from January 2013
684 to 2016-2017 winter in Beijing, China, Atmospheric Environment, 189, 133-144, 10.1016/j.atmosenv.2018.06.038,
685 2018.

686 Shi, X., and Brasseur, G. P.: The Response in Air Quality to the Reduction of Chinese Economic Activities during the
687 COVID-19 Outbreak, *Geophysical Research Letters*, 0-1, 10.1029/2020GL088070, 2020.

688 Si, Y. D., Wang, H. M., Cai, K., Chen, L. F., Zhou, Z. C., and Li, S. S.: Long-term (2006-2015) variations and relations
689 of multiple atmospheric pollutants based on multi-remote sensing data over the North China Plain, *Environmental
690 Pollution*, 255, 10.1016/j.envpol.2019.113323, 2019.

691 Sogacheva, L., Popp, T., Sayer, A. M., Dubovik, O., Garay, M. J., Heckel, A., Hsu, N. C., Jethva, H., Kahn, R. A.,
692 Kolmonen, P., Kosmale, M., de Leeuw, G., Levy, R. C., Litvinov, P., Lyapustin, A., North, P., Torres, O., and Arola,
693 A.: Merging regional and global aerosol optical depth records from major available satellite products, *Atmospheric
694 Chemistry and Physics*, 20, 2031-2056, 10.5194/acp-20-2031-2020, 2020.

695 Strode, S. A., Worden, H. M., Damon, M., Douglass, A. R., Duncan, B. N., Emmons, L. K., Lamarque, J.-F., Manyin,
696 M., Oman, L. D., Rodriguez, J. M., Strahan, S. E., and Tilmes, S.: Interpreting space-based trends in carbon monoxide
697 with multiple models, *Atmospheric Chemistry and Physics*, 16, 7285-7294, 10.5194/acp-16-7285-2016, 2016.

698 Sun, W., Shao, M., Granier, C., Liu, Y., Ye, C. S., and Zheng, J. Y.: Long-Term Trends of Anthropogenic SO₂, NO_x,
699 CO, and NMVOCs Emissions in China, *Earth's Future*, 6, 1112-1133, 10.1029/2018ef000822, 2018.

700 United Nations Environment Program (UNEP): *Independent Environmental Assessment: Beijing 2008 Olympic
701 Games*. Nairobi, Kenya, 2009.

702 Wang, M., Zhu, T., Zheng, J., Zhang, R. Y., Zhang, S. Q., Xie, X. X., Han, Y. Q., and Li, Y.: Use of a mobile laboratory
703 to evaluate changes in on-road air pollutants during the Beijing 2008 Summer Olympics, *Atmospheric Chemistry and
704 Physics*, 9, 8247-8263, 10.5194/acp-9-8247-2009, 2009.

705 Wang, P., Chen, K., Zhu, S., Wang, P., and Zhang, H.: Severe air pollution events not avoided by reduced
706 anthropogenic activities during COVID-19 outbreak, *Resources, Conservation and Recycling*, 158, 104814,
707 10.1016/j.resconrec.2020.104814, 2020.

708 Wang, P. C., Elansky, N. F., Timofeev, Y. M., Wang, G. C., Golitsyn, G. S., Makarova, M. V., Rakitin, V. S., Shtabkin,
709 Y., Skorokhod, A. I., Grechko, E. I., Fokeeva, E. V., Safronov, A. N., Ran, L., and Wang, T.: Long-Term Trends of
710 Carbon Monoxide Total Columnar Amount in Urban Areas and Background Regions: Ground- and Satellite-based
711 Spectroscopic Measurements, *Advances in Atmospheric Sciences*, 35, 785-795, 10.1007/s00376-017-6327-8, 2018.

712 Wang, T., Nie, W., Gao, J., Xue, L. K., Gao, X. M., Wang, X. F., Qiu, J., Poon, C. N., Meinardi, S., Blake, D., Wang,
713 S. L., Ding, A. J., Chai, F. H., Zhang, Q. Z., and Wang, W. X.: Air quality during the 2008 Beijing Olympics:
714 secondary pollutants and regional impact, *Atmospheric Chemistry and Physics*, 10, 7603-7615, 10.5194/acp-10-7603-
715 2010, 2010.

716 Wang, Y., and Wang, J.: Tropospheric SO₂ and NO₂ in 2012-2018: Contrasting views of two sensors (OMI and
717 OMPS) from space, *Atmospheric Environment*, 223, 10.1016/j.atmosenv.2019.117214, 2020.

718 Warner, J., Carminati, F., Wei, Z., Lahoz, W., and Attie, J. L.: Tropospheric carbon monoxide variability from AIRS
719 under clear and cloudy conditions, *Atmospheric Chemistry and Physics*, 13, 12469-12479, 10.5194/acp-13-12469-
720 2013, 2013.

721 Witte, J. C., Schoeberl, M. R., Douglass, A. R., Gleason, J. F., Krotkov, N. A., Gille, J. C., Pickering, K. E., and
722 Livesey, N.: Satellite observations of changes in air quality during the 2008 Beijing Olympics and Paralympics,
723 *Geophysical Research Letters*, 36, 10.1029/2009gl039236, 2009.

724 Xie, G. Q., Wang, M., Pan, J., and Zhu, Y.: Spatio-temporal variations and trends of MODIS C6.1 Dark Target and
725 Deep Blue merged aerosol optical depth over China during 2000-2017, *Atmospheric Environment*, 214,
726 10.1016/j.atmosenv.2019.116846, 2019.

727 Xu, J. H., Xie, H. M., Wang, K., Wang, J., and Xia, Z. S.: Analyzing the spatial and temporal variations in tropospheric
728 NO₂ column concentrations over China using multisource satellite remote sensing, *Journal of Applied Remote*
729 *Sensing*, 14, 10.11117/1.jrs.14.014519, 2020.

730 Yu, S. M., Yuan, J. G., and Liang, X. Y.: Trends and Spatiotemporal Patterns of Tropospheric NO₂ over China During
731 2005-2014, *Water Air and Soil Pollution*, 228, 10.1007/s11270-017-3641-9, 2017.

732 Yumimoto, K., Uno, I., and Itahashi, S.: Long-term inverse modeling of Chinese CO emission from satellite
733 observations, *Environmental Pollution*, 195, 308-318, 10.1016/j.envpol.2014.07.026, 2014.

734 Zhang, Y., Li, C., Krotkov, N. A., Joiner, J., Fioletov, V., and McLinden, C.: Continuation of long-term global SO₂
735 pollution monitoring from OMI to OMPS, *Atmospheric Measurement Techniques*, 10, 10.5194/amt-10-1495-2017,
736 2017.

737 Zhao, Y., Nielsen, C. P., McElroy, M. B., Zhang, L., and Zhang, J.: CO emissions in China: Uncertainties and
738 implications of improved energy efficiency and emission control, *Atmospheric Environment*, 49, 103-113,
739 10.1016/j.atmosenv.2011.12.015, 2012.

740 Zhao, Y., Zhang, J., and Nielsen, C. P.: The effects of recent control policies on trends in emissions of anthropogenic
741 atmospheric pollutants and CO₂ in China, *Atmospheric Chemistry and Physics*, 13, 487-508, 10.5194/acp-13-487-
742 2013, 2013.

743 Zheng, B., Chevallier, F., Ciais, P., Yin, Y., Deeter, M. N., Worden, H. M., Wang, Y. L., Zhang, Q., and He, K. B.:
744 Rapid decline in carbon monoxide emissions and export from East Asia between years 2005 and 2016, *Environmental*
745 *Research Letters*, 13, 10.1088/1748-9326/aab2b3, 2018a.

746 Zheng, B., Tong, D., Li, M., Liu, F., Hong, C. P., Geng, G. N., Li, H. Y., Li, X., Peng, L. Q., Qi, J., Yan, L., Zhang,
747 Y. X., Zhao, H. Y., Zheng, Y. X., He, K. B., and Zhang, Q.: Trends in China's anthropogenic emissions since 2010 as
748 the consequence of clean air actions, *Atmospheric Chemistry and Physics*, 18, 14095-14111, 10.5194/acp-18-14095-
749 2018, 2018b.

750

751 **Tables**

752

753 **Table 1. Summary statistics for central east China comparing 2020 and 2019 during January 23 – April 8.**

Variable	2020 mean	2020 % difference	
		2019 mean	from 2019
CO	133.5	137.9	-3.2
(ppbv)	(130.3, 136.8)	(134.7, 141.3)	(-6.3, 0.1)
SO₂	0.057	0.031	95
(DU)	(0.045, 0.070)	(0.018, 0.046)	(14.8, 249.6)
NO₂	6.5	9.6	-32.1
(10 ¹⁵ molec cm ⁻²)	(5.8, 7.2)	(8.7, 10.5)	(-42.1, -21.7)
AOD	0.41	0.48	-14.3
	(0.36, 0.46)	(0.41, 0.55)	(-29.4, 3.1)

754

755

Table 23. Same as Table 1, but for southern China.

Variable	2020 mean	2019 mean	2020 %	
			difference	
CO	144.7	128.5	12.6	from 2019
(ppbv)	(139.6, 150.3)	(124.4, 132.8)	(7.2, 18.3)	
SO₂	0.003	-0.020	116	
(DU)	(-0.01, 0.020)	(-0.04, -0.001)	(24, 223)	
NO₂	3.3	4.3	-22.2	
(10 ¹⁵ molec cm ⁻²)	(3.0, 3.7)	(3.9, 4.7)	(-32.6, -10.4)	
AOD	0.38	0.34	12	
	(0.34, 0.43)	(0.30, 0.39)	(-7, 34)	

758
 759 **Table 35.** 2014 anthropogenic emissions estimates by sector (in %) over China, excluding biomass burning, from the
 760 Community Emissions Data System (CEDS) for a representative set of constituents: black carbon (BC), carbon monoxide
 761 (CO), ammonia (NH₃), nitrogen oxides (NO_x), organic carbon (OC) and sulfur dioxide (SO₂). Residential, commercial and
 other sectors are combined as RCO.

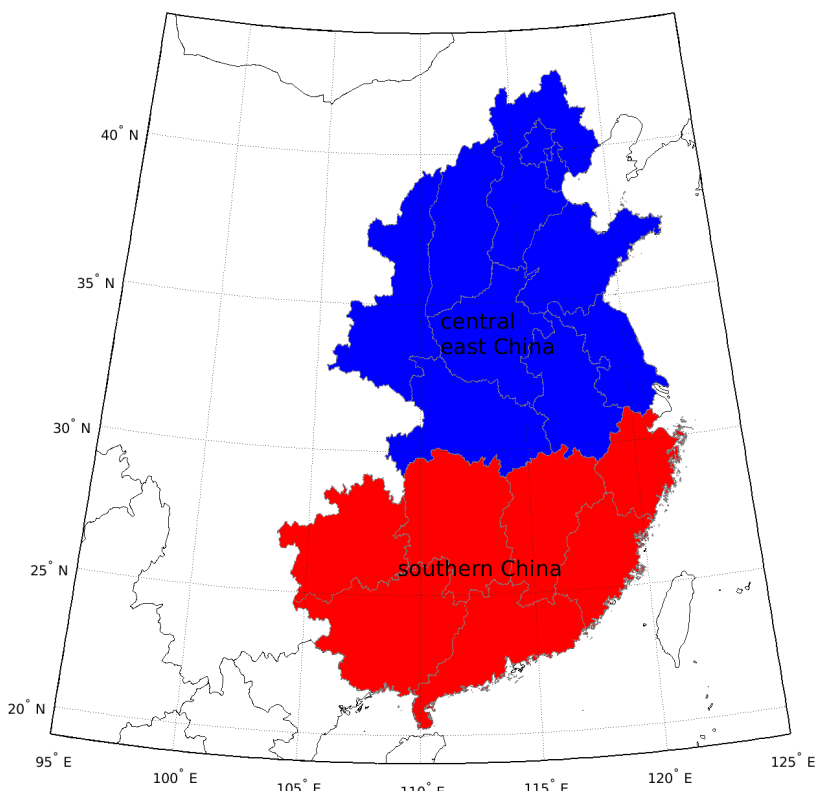
	BC	CO	NH ₃	NOx	OC	SO ₂
Agriculture	0	0	61.6	1.1	0	0
Energy	32.6	8	0.4	38.5	28.3	29.4
Industrial	12.7	41.8	6.5	33	5.1	57.3
Ground transportation	8.1	7.2	0.5	17.5	1.7	0.3
RCO	38.1	36.7	5.2	4.2	38.4	12.5
Solvents	0	0	0	0	0	0
Waste	8.5	6.3	25.8	5.2	26.5	0.4
Shipping	0	0	0	0.2	0	0.1
Aircraft	0	0	0	0.2	0	0

762

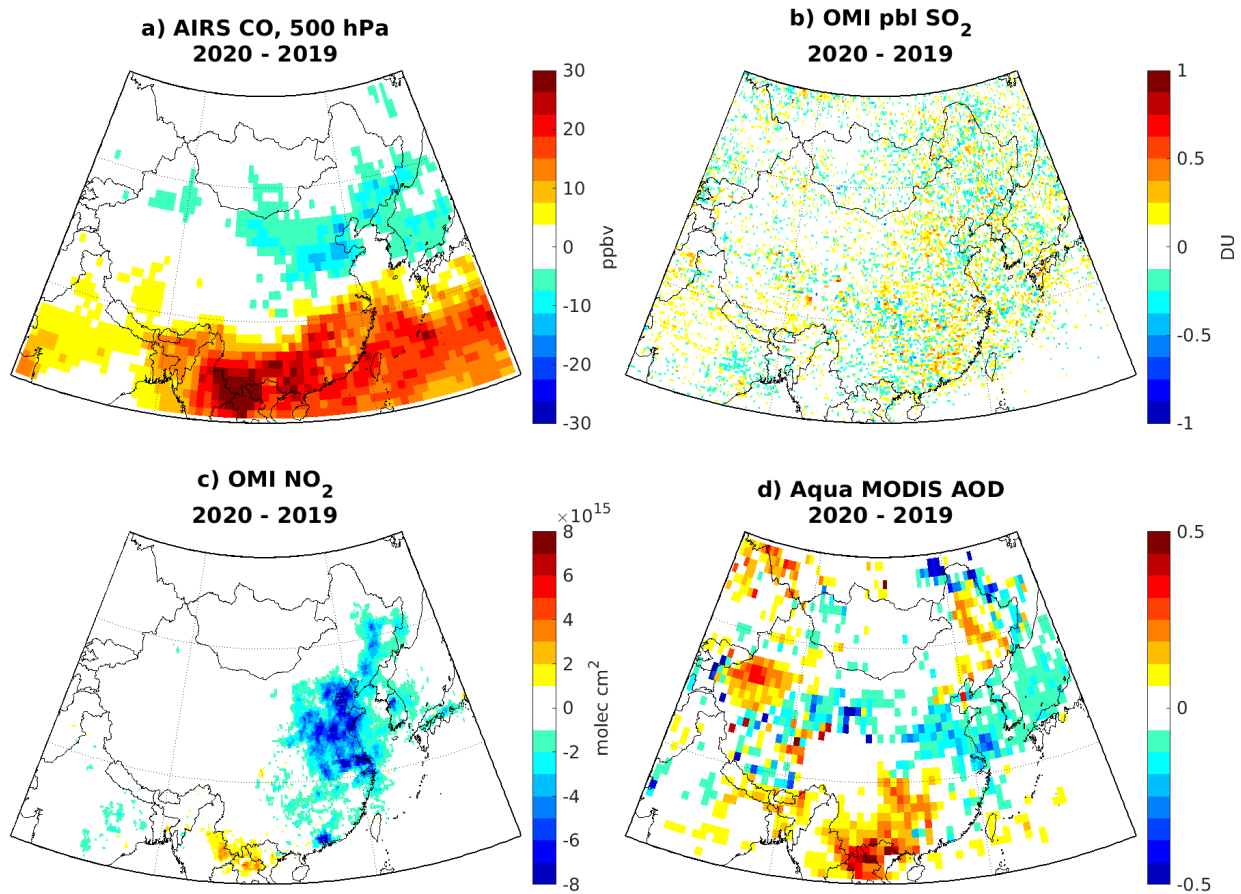
763
 764 **Table 46. Bottom up biomass Global Fire Assimilation System (Kaiser et al., 2012) burning CO emissions estimates from**
 765 **the Upper Mekong region (17° N to 24° N, 95° E to 105° E) and AIRS CO over southern China from January 23 to April 8,**
for 2005-2020.

Year	GFAS CO Upper Mekong (KT)	AIRS CO southern China 500 hPa (ppbv)
2005	7977	157
2006	8905	146
2007	15734	165
2008	4542	153
2009	9990	140
2010	14176	149
2011	3591	147
2012	11320	153
2013	8684	145
2014	8722	142
2015	8084	143
2016	9642	149
2017	3736	131
2018	3179	139
2019	6309	128
2020	7871	145

766

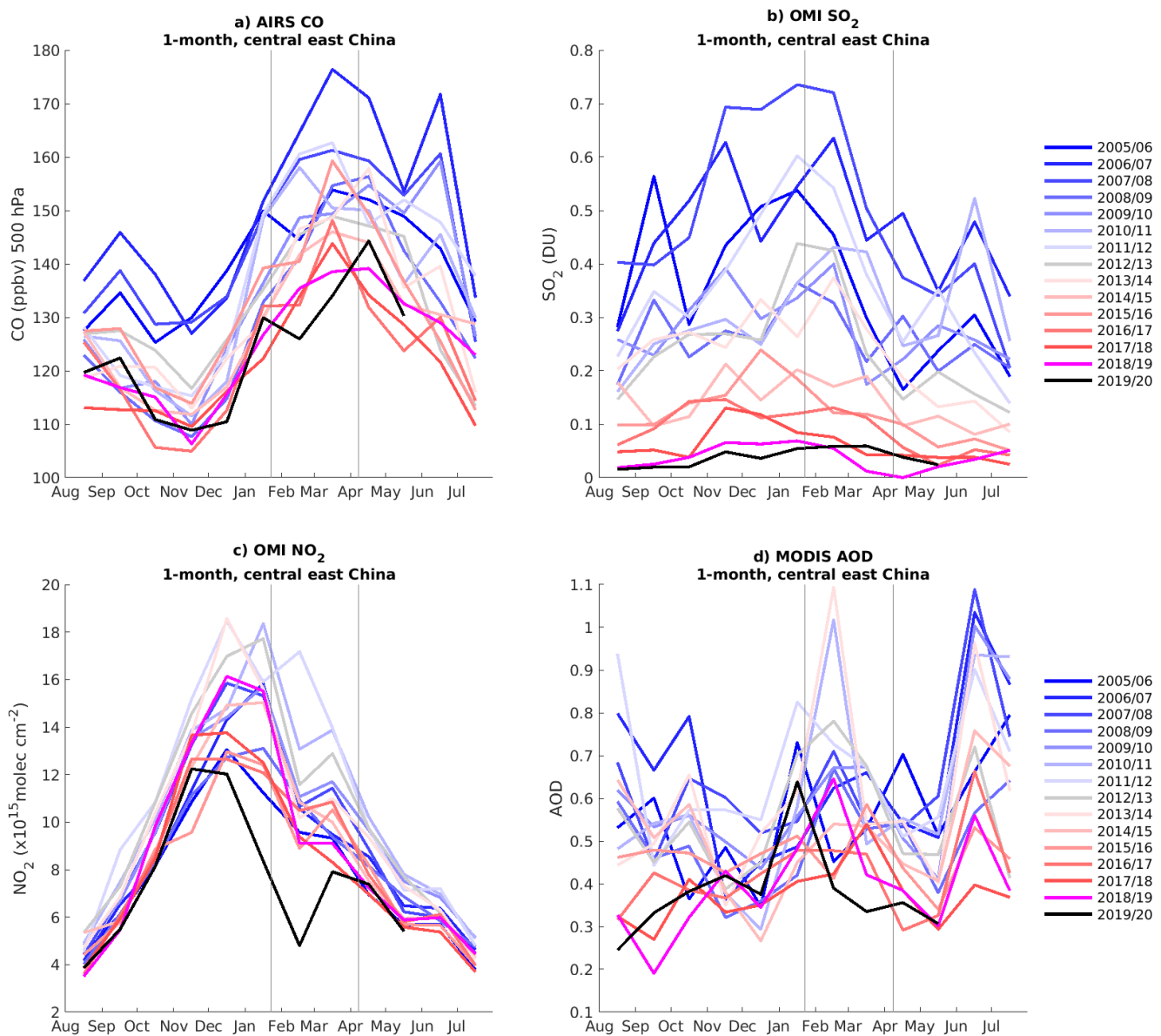


769 **Figure 1. Groupings of provinces for central east China and southern China.**

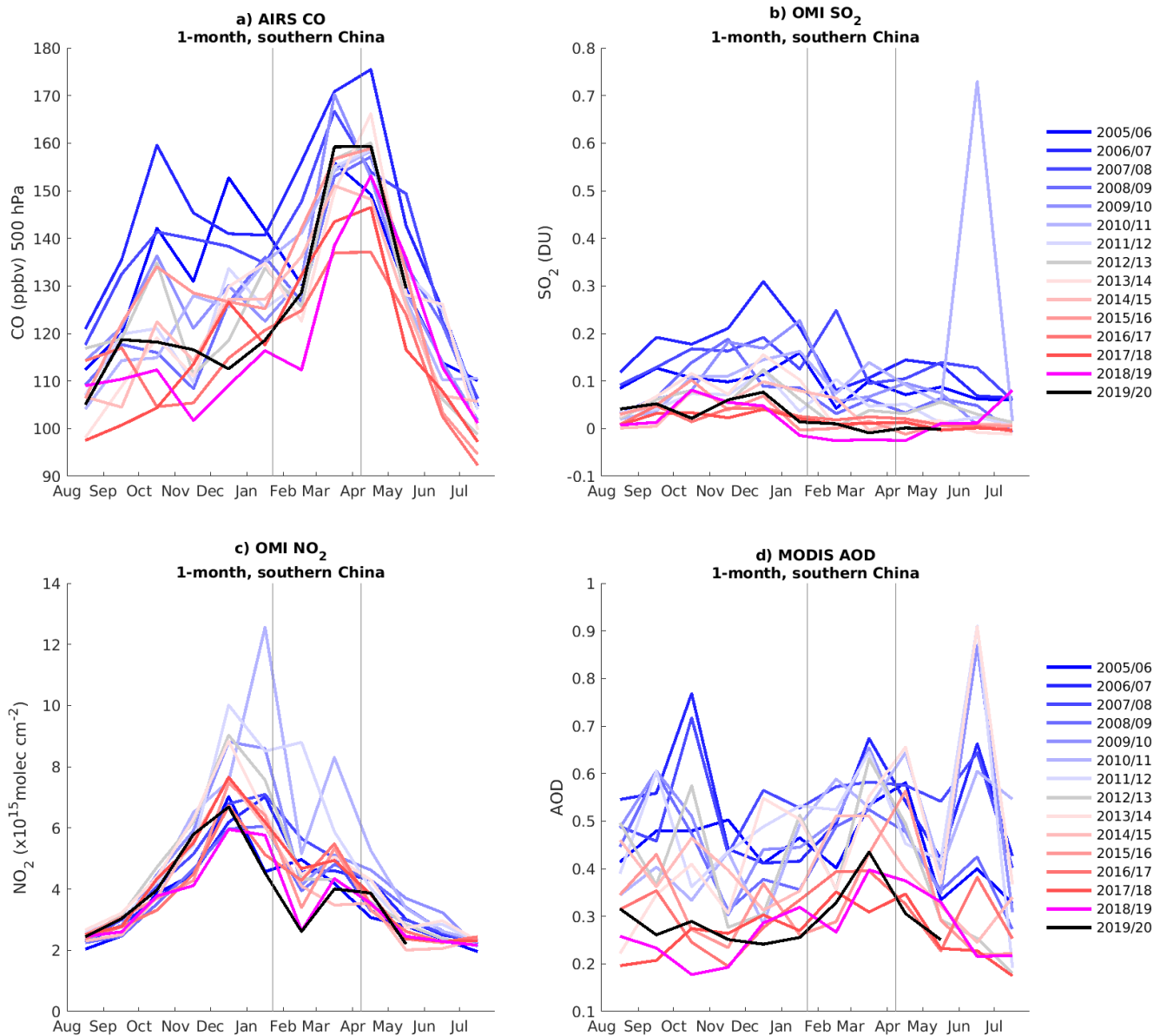


770

771 **Figure 2. 2020-2019 differences during January 23 to April 8 over China in a) AIRS carbon monoxide (CO) at 500 hPa, b)**
 772 **OMI PBL sulfur dioxide (SO₂), c) OMI tropospheric nitrogen dioxide (NO₂) and d) Aqua MODIS aerosol optical depth**
 773 **(AOD).**



775 **Figure 3.** Monthly mean a) AIRS CO, b) OMI PBL SO_2 , c) OMI tropospheric NO_2 and d) MODIS AOD over central east China since 2005. As in Bauwens et al. (2020), each year starts in August to show any departure from the seasonal cycle during the January 23 to April 8 lockdown period, shown by the thin grey vertical lines.



780 **Figure 4.** Same as [Figure 3](#), but for southern China.

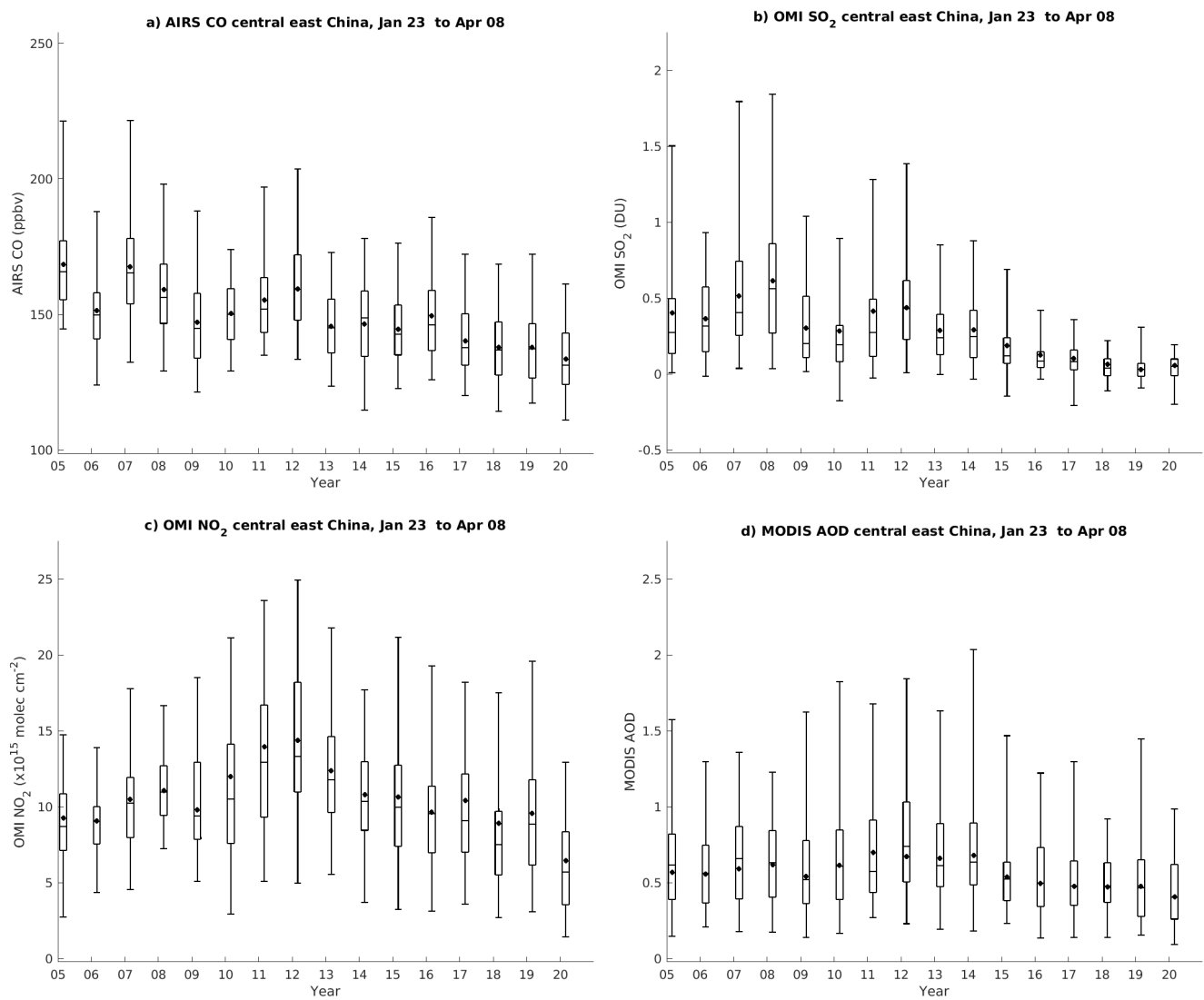


Figure 5. January 23-April 8 box plots over central East China for a) AIRS CO, b) OMI PBL SO₂, c) OMI tropospheric NO₂ and d) Aqua and Terra MODIS AOD from 2005 to 2020. The black box plots show the median, interquartile range and 2.5th and 97.5th percentiles over all daily data, with the mean shown by the black dot.

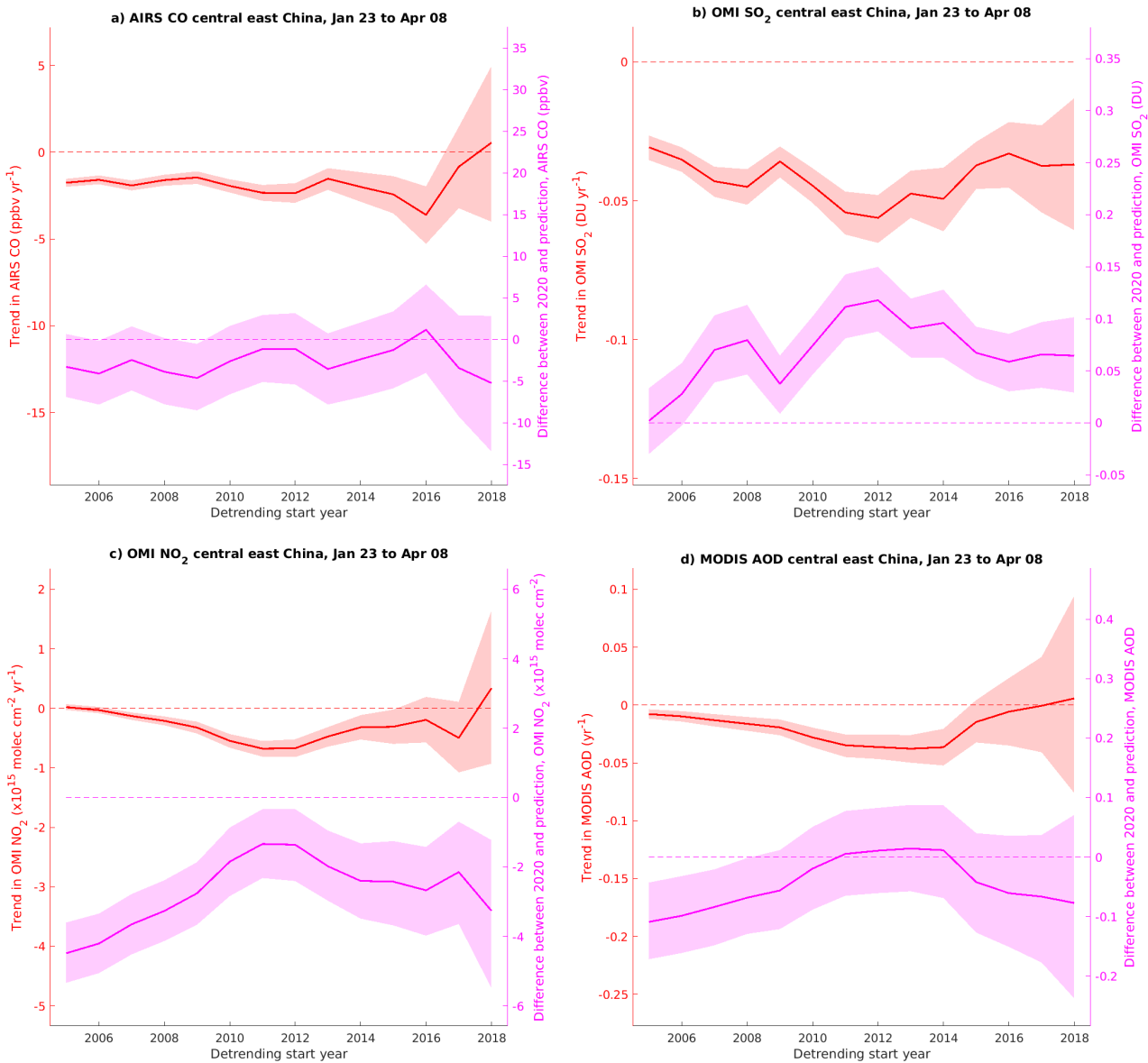
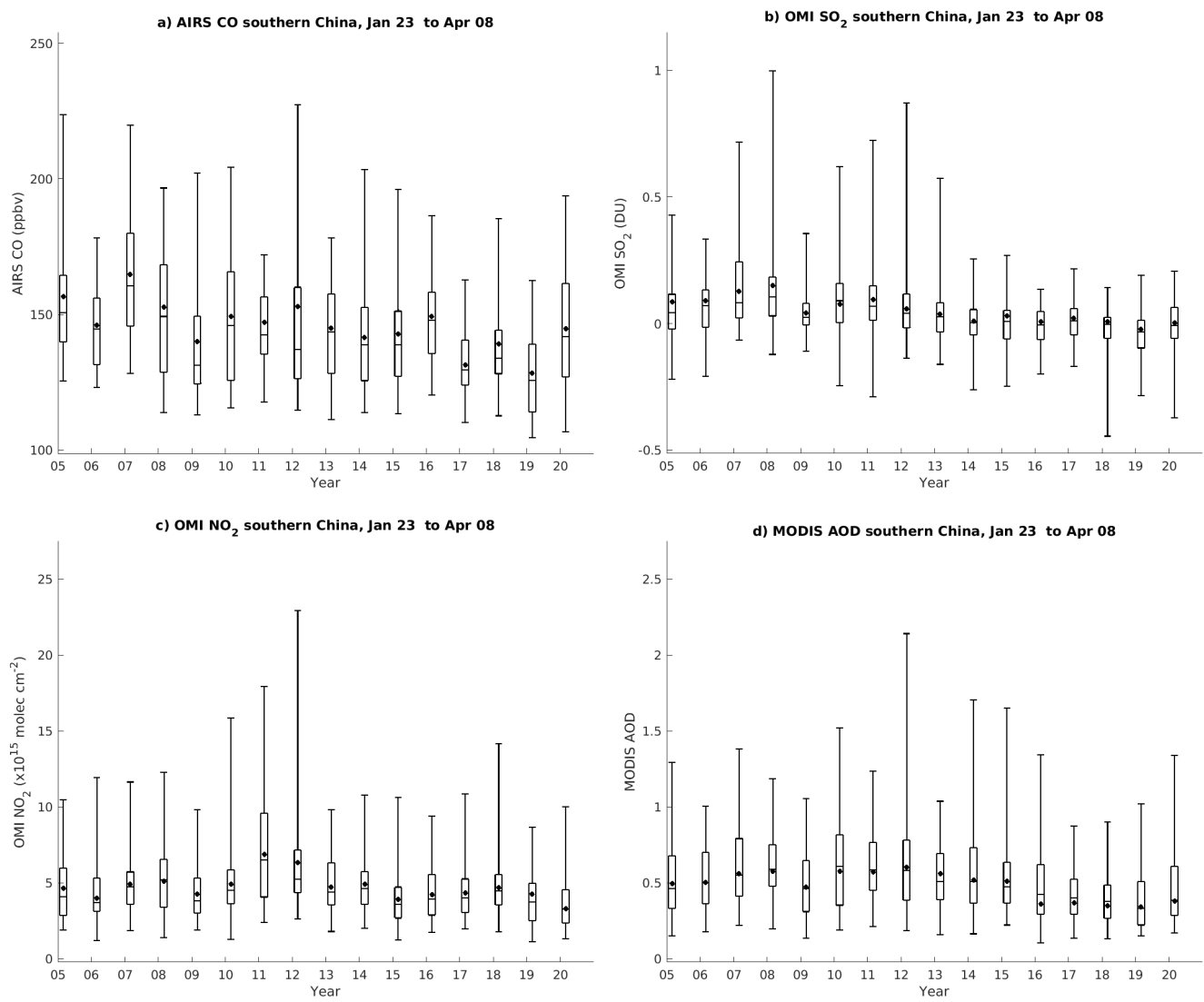


Figure 6. Dependence of trends (red) and difference between 2020 observations and predicted value (magenta) on detrending start year over central east China for a) AIRS CO, b) OMI PBL SO₂, c) OMI tropospheric NO₂ and d) MODIS AOD. The solid line shows the mean of the estimate for each year and the shading shows the 95% confidence interval.



790 **Figure 7.** Same as Figure 5 but for southern China.

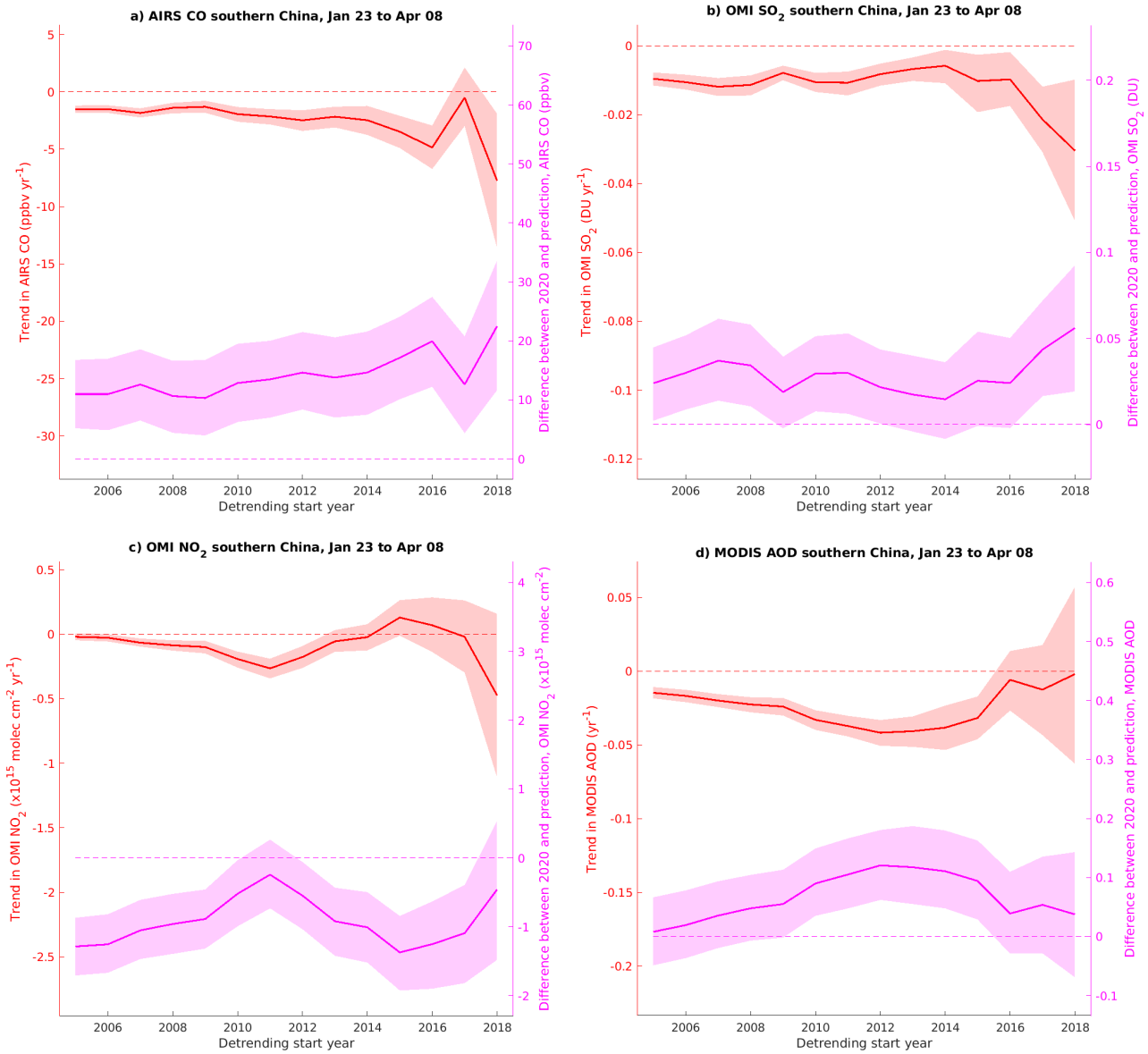


Figure 8. Same as Figure 6, but for southern China.